



Graz University of Technology in Cooperation with the German Research Center
Heidelberg

Overexpression of ISL1 in adult Neural Stem Cells by using an Adeno Associated Virus

Master Thesis

Submitted to the
Institute of Molecular Biotechnology
Graz University of Technology

by

Alexander Laure, B.Sc.

Declaration

This Master Thesis was written at the German Cancer Research Center (DKFZ) in close collaboration with the Graz University of Technology in the period from June 2017 to December 2017 under the direct supervision of **Prof. Dr. Ana Martin-Villalba** (DKFZ - Molecular Neurobiology).

1st Examiner

Univ.-Prof.i.R. Dipl.-Ing. Dr.tech

Helmut Schwab

Institute of Molecular Biotechnology

Graz University of Technology

I, Alexander Laure herewith declare that I wrote this Master Thesis independently, under supervision, and that I used no other sources and aids than those indicated throughout the thesis.

Klagenfurt, 21.03.2017

Place, Date

Signature

Acknowledgement

This Master project was accomplished in the period from April 2017 to Dezember 2017 in the molecular neurobiology Department of the German Cancer Research Center (DKFZ) in Heidelberg and the Institute of Molecular Biotechnology at the Graz University of Technology with the contribution of many people.

First and foremost, I would like to express my utmost gratitude to my supervisors Prof. Dr. Ana Martin-Villalba (DKFZ), Sascha Dehler, MSc (DKFZ) and Univ.-Prof.i.R. Dipl.-Ing. Dr.tech Helmut Schwab (TUG) for giving me the opportunity to work on this thesis. Prof. Martin-Villalba initiated and provided me this exciting project to work on and supported me constantly with guidance throughout this study.

My greatest thanks belong to Sascha for teaching me everything about mice and how to handle those little creatures and always being patient and encroaching. Further, I would like to thank everyone from the Neurolab, especially Birgit, Georgios, Nikhil, Oguzhan, Suse and Maxim for interesting and helpful discussions, assistance in the lab and the few after work beers.

In addition, I am very thankful to Prof. Helmut Schwab for taking over the supervision of this thesis on the part of the Graz University of Technology and being so patient.

I am more than thankful for all the new friends and flat mates I have met in Heidelberg, as well as everyone from home who came to visit me for their encouragement and friendship, for drinking coffee and gin, having lunch together, getting through tough days and so much more. Special thanks go to the person who persuaded me to come to Heidelberg.

Finally, I would like to deeply thank the ones I love for their selfless and constant support during all periods of my life. They have been there through good and bad. There are no words that could express how much they mean to me!

Table of contents

1	INTRODUCTION	- 1 -
1.1	NEUROGENESIS	- 1 -
1.1.1	<i>Developmental neurogenesis</i>	- 1 -
1.1.2	<i>Adult neurogenesis</i>	- 2 -
1.1.3	<i>Injury induced neurogenesis</i>	- 5 -
1.2	ISL1	- 7 -
1.3	ADENO-ASSOCIATED VIRUS	- 8 -
1.3.1	<i>Characteristics of AAVs</i>	- 9 -
1.3.2	<i>Production</i>	- 10 -
1.3.3	<i>Designer AAVs</i>	- 12 -
1.4	AIM OF THE PROJECT	- 13 -
2	MATERIAL AND METHODS.....	- 14 -
2.1	MATERIALS	- 14 -
2.1.1	<i>Reagents</i>	- 14 -
2.1.2	<i>Buffers and media</i>	- 17 -
2.1.3	<i>Antibodies</i>	- 20 -
2.1.4	<i>Primer</i>	- 22 -
2.2	METHODS.....	- 23 -
2.2.1	<i>Adeno Associated virus</i>	- 23 -
2.2.2	<i>In vitro experiments</i>	- 25 -

2.2.3	<i>In vivo experiments</i>	- 28 -
3	RESULTS	- 32 -
3.1	TRANSPLANTATION.....	- 32 -
3.1.1	<i>Infection efficiency in vitro</i>	- 33 -
3.1.2	<i>Isl1 Expression</i>	- 34 -
3.1.3	<i>Transplantation of Isl1 infected cells</i>	- 35 -
3.2	DIRECT INJECTION.....	- 38 -
3.2.1	<i>Infection efficiency in vivo</i>	- 38 -
3.2.2	<i>Direct injection of Isl1 to the ventricle</i>	- 41 -
4	DISCUSSION	- 43 -
4.1	AAV EFFICIENCY	- 43 -
4.2	TRANSPLANTATION.....	- 44 -
4.3	DIRECT INJECTION.....	- 45 -
	REFERENCES	- 47 -

List of figures

- Figure 1** The NSC lineage within the V-SVZ
- Figure 2** Regional origins of NSCs within the V-SVZ
- Figure 3** Adeno-associated virus (AAV) structure
- Figure 4** Recombinant Adeno associated virus (AAV) production using the triple-plasmid transfection method
- Figure 5** Proposed model for the molecular regulation of injury-induced fate plasticity
- Figure 6** Genetic background of the reporter system
- Figure 7** Infection efficiency assay in vitro
- Figure 8** Isl1 transcription and expression levels
- Figure 9** Scheme of the transplantation experimental design
- Figure 10** FACS sorting strategy for NSCs from the V-SVZ
- Figure 11** Confocal images of Isl1 infected NSCs 5 weeks after transplantation
- Figure 12** Scheme of the direct injection experimental design
- Figure 13** Confocal images of AAV1_P5 injected ventricles 5 days post injection
- Figure 14** Celltype quantification of AAV1_P5 infected cells
- Figure 15** Confocal images 5 weeks after of directly injecting an Isl1 overexpressing AAV1_P5 into the ventricle

List of tables

Table 1	Chemicals, Kits and Reagents
Table 2	Antibodies for IHC, Western Blots and FACS
Table 3	Primer for AAV Titration, Expression qPCR and reverse transcription
Table 4	qPCR setup for AAV titration
Table 5	Reverse transcription mix
Table 6	Cycling conditions for reverse transcription
Table 7	Cycling conditions for DNA amplification
Table 8	Celltype specific markers for quantification of in vivo infection efficiency

Abbreviations

Abbreviation	Description
AAV	Adeno-associated virus
Ad	Adenovirus
aNSC	Active neural stem cell
BCCAO	Bilateral common carotid artery occlusion
BLBP	Brain lipid-binding protein
CNS	Central nervous system
CSF	Cerebrospinal fluid
DG	Dentate gyrus
DMR	Differentially methylated region
EGF	Epidermal growth factor
FACS	Fluorescence activated cell sorting
FGF	Fibroblast growth factor
GAP	GTPase activating protein
GC	Granule cell
GFAP	Glial fibrillary acidic protein
GLAST	Glutamate aspartate transporter
HEK cells	Human embryonic kidney cells
IHC	Immunohistochemistry
IPC	Intermediate progenitor cells
ITR	Inverted terminal repeat
MOI	Multiplicity of infection
NB	Neuroblast
Ng2	Neurogenin-2

NSC	Neural stem cell
OB	Olfactory bulb
ORF	Open reading frame
PGC	Periglomerular cells
qNSC	Quiescent neural stem cell
RMS	Rostral migratory stream
SGZ	Subgranular zone
TAP	Transit-amplifying progenitor
TdTom	TdTomato
V-SVZ	Ventricular-Subventricular zone
Wt	Wild-type

Abstract

Neurogenesis describes the process of neuronal birth and is based on the presence of only one subtype of cells called neural stem cells. Over the last decades, many studies demonstrated that neurogenesis is not only limited to the developing brain, but also takes place in the adult mammalian brain. In the ventricular-subventricular zone, neural stem cells are mainly generating neuronal precursor cells that migrate into the olfactory bulb under homeostatic conditions. Upon injury neural stem cells have the capability to send precursor cells into lesioned areas of the striatum. However, the capacity for brain regeneration is fairly limited. The epigenetic landscape, here DNA methylation, seems to play a significant role in regulating injury induced neurogenesis. Recent studies in the Ana Martin-Villalba laboratory identified the transcription factor ISL1 as a possible candidate to bind to demethylated regions in the Epigenome of neural stem cells in mice with ischemic injury.

Here, we successfully generated an Isl1 overexpressing adeno associated virus, that specifically targets cells in the neural stem cell containing walls of the lateral ventricle. Further, cellular and molecular characteristics of Isl1 overexpression in adult neural stem cells was analyzed in vitro and in vivo.

This study reveals a potential strategy to repopulate the injury site upon ischemia and may open potential strategies for regenerative medicine within the adult brain.

Zusammenfassung

Neurogenese beschreibt den Prozess der neuronalen Entwicklung und basiert auf nur einem Subtyp von Zellen, den neuralen Stammzellen. In den letzten Jahrzehnten haben viele Studien gezeigt, dass die Neurogenese nicht nur auf das sich entwickelnde Gehirn beschränkt ist, sondern auch im erwachsenen Säugetiergehirn stattfindet. In der ventrikulär-subventrikulären Zone produzieren neurale Stammzellen hauptsächlich neuronale Vorläuferzellen, die unter homöostatischen Bedingungen in die Bulbus olfactorius wandern. Nach einer Verletzung haben neurale Stammzellen die Fähigkeit, Vorläuferzellen in lädierte Bereiche des Striatums zu senden. Die Fähigkeit zur Regeneration des Gehirns ist jedoch ziemlich begrenzt. Die epigenetische Landschaft, hier die DNA-Methylierung, scheint eine bedeutende Rolle bei der Regulierung der verletzungsinduzierten Neurogenese zu spielen. Jüngste Studien im Labor von Ana Martin-Villalba identifizierten den Transkriptionsfaktor ISL1 als möglichen Kandidaten für die Bindung an demethylierte Regionen im Epigenom neuraler Stammzellen bei Mäusen mit ischämischer Schädigung.

Hier konnten wir erfolgreich ein Is11-überexprimierendes Adeno-assoziiertes Virus generieren, das spezifisch auf neurale Stammzellen in den Wänden des lateralen Ventrikels zielt. Weiter wurden die zellulären und molekularen Eigenschaften der Is11-Überexpression in adulten neuralen Stammzellen *in vitro* und *in vivo* analysiert.

Diese Studie zeigt eine mögliche Strategie auf, um die Läsionen nach Ischämie neu zu bevölkern und könnte potentielle Strategien für die regenerative Medizin im erwachsenen Gehirn eröffnen.

1 Introduction

1.1 Neurogenesis

The human brain is often compared with a supercomputer. It is able to perform multiple, highly complicated tasks simultaneously. To achieve this, about 85 billion neurons are working together with the same number of assisting cells (Azevedo et al., 2009). The cells responsible for transmitting information with electric signals within the brain, the neurons, occur in a variety of different subtypes, regarding their molecular, structural and functional identity. Glial cells are responsible to support the neurons metabolism, the immune system and the transmission of information. They mainly occur in three different subtypes, astrocytes, micro-glia and oligodendrocytes (Tanaka and Ferretti, 2009).

Upon brain injuries, the capacity for self-repair is fairly limited. One reason might be the complex structure and organization of the adult brain. To understand the regeneration upon tissue damage in the adult brain, it is important to get insight into the process of adult neurogenesis under injury conditions.

1.1.1 Developmental neurogenesis

In the mouse, brain development starts between gestational day 7 and 9 (E7-9). The ectodermal neural tube forms neuroepithelial cells that undergo several rounds of symmetric divisions to increase their number. From E9-10, these neuroepithelial cells transform to so called radial glia (RG). RG are the origin of almost all, if not all, astrocytes, neurons and oligodendrocytes in the CNS, generated during development. Often called neural stem cells (NSCs) of the embryonic brain (Götz and Barde, 2005). The term glia is used due to the astroglial cell properties like the expression of the astrocyte specific glutamate aspartate transporter (GLAST), brain lipid-binding protein (BLBP) and intermediate filaments like nestin (Kriegstein and Alvarez-buylla, 2011). RG divide mostly asymmetrically maintain self-renewal and to generate intermediate progenitor cells (IPCs) that populate an arising subventricular zone (SVZ). IPCs differentiate either directly into neurons or after a number of symmetric divisions to first increase their own number (Kriegstein and Alvarez-buylla, 2011). To reach their final place in the cortical plate, newly differentiated neurons migrate along the radial process

of the RG. The final neuron subtype is determined by a combination of temporal and spatial cues (Custo Greig et al., 2013).

1.1.2 Adult neurogenesis

In most brain areas, developmental neurogenesis ends after the early postnatal period. However, in two main regions of the adult brain, a certain NSC population is kept throughout life. These brain compartments are the subgranular zone (SGZ) of the hippocampal dentate gyrus (DG) and the ventricular-subventricular zone (V-SVZ) of the lateral ventricle. Here, NSCs proliferate and give rise to new neurons, a process referred as adult neurogenesis.

Historically, it was believed for a long time, that the amount of neurons is fixed in the adult brain, and no neurogenesis occurs after the postnatal period (Kempermann et al., 2006). However, already in the early 20th century, Allen postulated that neurogenesis continues throughout life (Allen, 1912). The link between cell proliferation and generation of new neurons in the adult brain was made by Joseph Altman, first in the hippocampus (Altman, 1963), and some years later in the V-SVZ (Altman, 1969). By today, it is well known, that the adult brain harbors stem cells with the capacity of self-renewal and differentiation like most other tissues in mammals (Bergmann et al., 2012; Ernst et al., 2014). NSCs from the V-SVZ differentiate into olfactory neurons. Their main functions are circuit plasticity and odor discrimination (Lledo et al., 2008). Other than V-SVZ NSCs, neural stem cells from the SGZ give rise to granule neurons in the DG. Their main functions are memory, mood and learning (Ming and Song, 2011). As this thesis will mainly focus on V-SVZ NSCs, their cellular and functional properties will be explained in more detail.

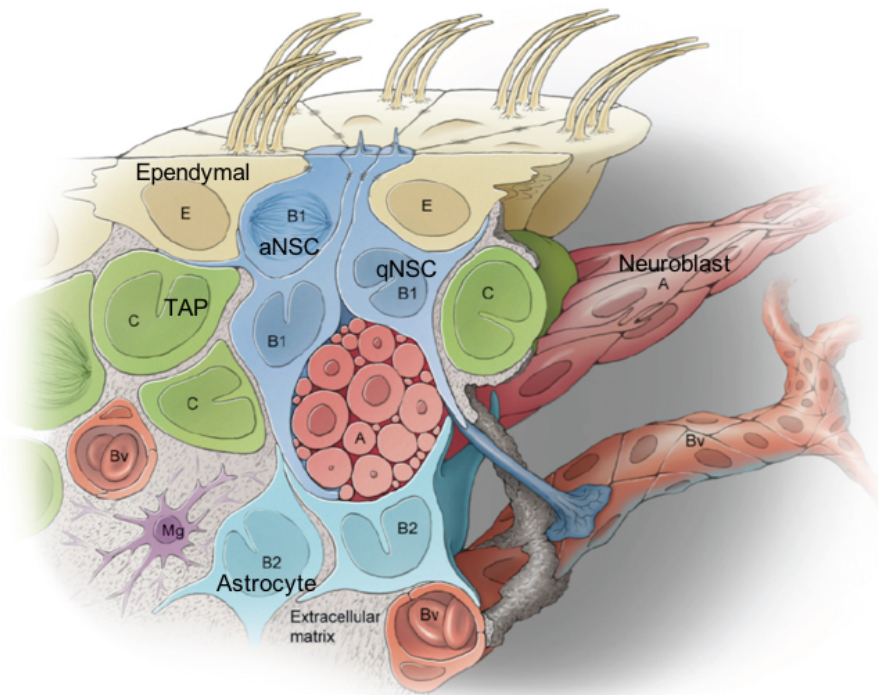


Figure 1 The NSC lineage within the V-SVZ. Schematic view of the Ventricular-Subventricular Zone with the main cell types involved. Quiescent neural stem cells become active NSC to then divide into transit amplifying cells. After division, TAPs become neuroblasts and migrate along the rostral migratory stream towards the olfactory bulbs. E., Ependymal cell; Bv., Blood vessel; Mg., Microglia. Adapted from (Ihrie and Álvarez-Buylla, 2011).

The SVZ-NSCs are organized in a pinwheel like structure (**Figure 1**). Quiescent neural stem cells (qNSCs) have apical processes to interact with the cerebrospinal fluid (CSF) in the ventricle. To receive signals from the blood stream, they have long basal, cytoplasmic processes to interact with blood vessels (Doetsch et al., 1997). Most NSCs in the V-SVZ are in a non-dividing quiescent state. It was suggested that at any given time about 8% of all NSCs exit the quiescent state to enter the cell cycle to maintain the NSC pool. These cells are referred to as active NSCs (aNSCs) (Ponti et al., 2013). More recent studies suggest that the vast majority of qNSCs divide symmetrically, whereas 20-30% symmetrically self-renew and can remain in their niche for several months before differentiating. 70-80% undergo consuming division to generate progeny (Obernier et al., 2018). However, the self-renewal capacity of NSCs drops with the number of NSCs within the same niche (Basak et al., 2018).

Single cell RNA sequencing revealed that the transition from qNSC to aNSC involves at least three steps. Dormant or qNSC1 cells get activated upon certain cell signals or after

a brain injury and become primed quiescent or qNSC2. Upon further lineage progression, they become aNSC1 and are able to enter the cell cycle as active dividing or aNSC2. During this lineage progression, the cell metabolism changes drastically (Llorens-Bobadilla et al., 2015).

aNSCs divide to generate transit amplifying cells (TAPs). TAPs lose their processes towards the ventricle and blood vessels (Ihrie and Álvarez-Buylla, 2011; Obernier et al., 2018). They further divide symmetrically to generate more TAPs or differentiate into neuroblasts (NBs). NBs further divide and gather in chains through which they migrate tangentially towards the olfactory bulbs (OB). The migration path is referred to as rostral migratory stream (RMS) (Lledo et al., 2006; Lois et al., 1996; Massalini et al., 2009). After the NB reaches the OB, it migrates to different positions within the granule cell layer and the glomeruli to differentiate into various olfactory interneuron types, depending on the origin within the V-SVZ (**Figure 2**) (Lim and Alvarez-Buylla, 2014; Lledo et al., 2008).

Dorsal NSCs differentiate to superficial granule cells (GCs) and anterior TH-positive periglomerular cells (PGCs). Ventral NSCs produce deep GCs and calbindin-positive periglomerular cells. Other regions of the V-SVZ, like the dorsal wall facing the cortex and the medial wall facing the septum or aNSCs from within the RMS, form different types of interneurons in the OBs (Alonso et al., 2008; Kohwi et al., 2007; Merkle et al., 2013). It has been shown, that isolated NSCs from one area of the V-SVZ can be transplanted to another area and still produce interneurons from the original origin. For example, ventral NSCs transplanted into the V-SVZ still produce calbindin-positive, but not TH-positive PGCs (Lim and Alvarez-Buylla, 2014).

By today, it remains unclear how many regions exist in the V-SVZ and how many different types of interneurons can be produced in the adult mammalian brain. However, it is clearly understood that the V-SVZ is subdivided into different regions that produce different types of interneurons and GCs.

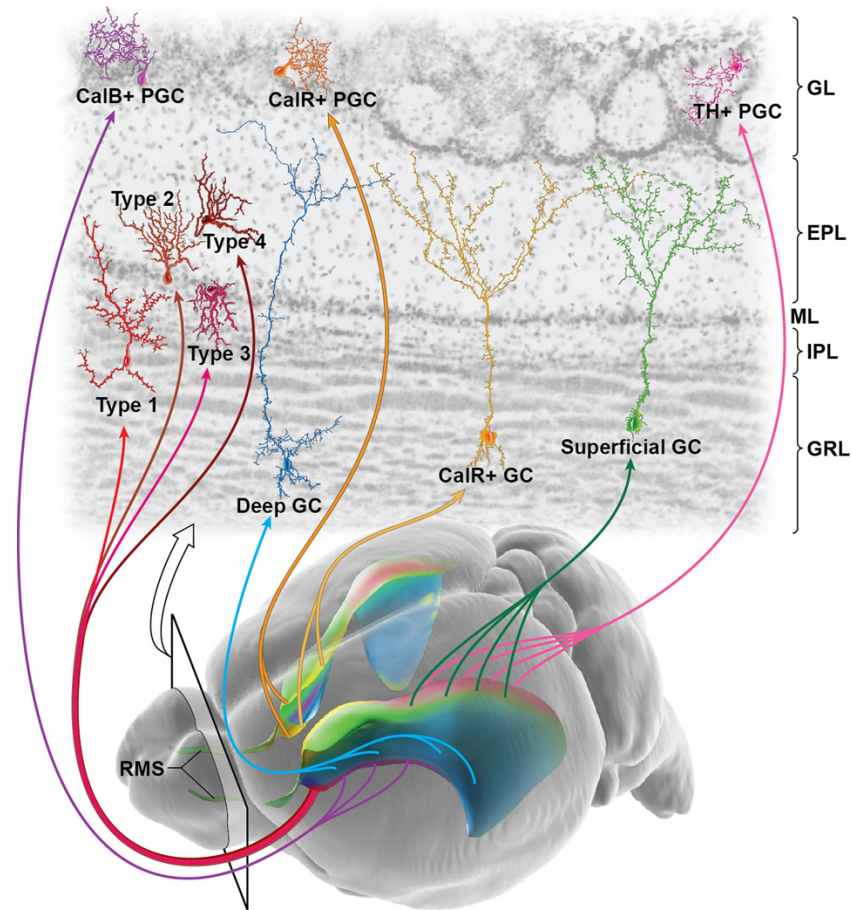


Figure 2 Regional origins of NSCs within the V-SVZ. Schematic view of the adult mouse brain with colorized lateral ventricles. Neural stem cells (NSCs) from the Ventricular-Subventricular zone (V-SVZ) differentiate and migrate towards the rostral migratory stream (RMS) to give rise to certain olfactory bulb (OB) interneurons. The type of OB interneuron depends on the origin of the NSC within the V-SVZ. CalB., calbindin; CalR., calretinin; TH., tyrosine hydroxylase; PGC., periglomerular cell; GC., granule cell; GL., glomerular layer; EPL., external plexiform layer; ML., mitral cell layer; IPL., internal plexiform layer; GRL., granular layer. Adapted from (Lim and Alvarez-Buylla, 2014).

1.1.3 Injury induced neurogenesis

The regenerative capacity of the adult mammalian brain is fairly limited, and the rate of self-repair is very low compared to other organs such as heart, liver, peripheral nervous system (Kyritsis et al., 2014). Non-mammalian species such as teleost fish and amphibians show higher brain repair capacities (Tanaka and Ferretti, 2009). However, some tissue repair mechanisms are activated after brain injuries to narrow the brain damage and retain crucial brain functions. This repair can be referred to as injury induced neurogenesis.

Under homeostatic condition, new neurons are generated to a constant level. Upon injury, certain NSC containing brain regions, such as the V-SVZ, are able to upregulate neurogenesis and provide new neurons for brain repair mechanisms (Nakafuku and Grande, 2013). After ischemic brain damage in the striatum, it has been shown that new neurons derive from the V-SVZ and migrate to the injured areas (Arvidsson et al., 2002; Collin et al., 2005). By today, various studies have shown the capacity of the adult mammalian brain to replace damaged neurons after injuries. There are studies for a variety of injury models and brain regions (Nakafuku and Grande, 2013).

This repair mechanisms are relatively poor without other stimuli, as only a small amount of injured neurons will be replaced after injury (Collin et al., 2005). The production of specific neuronal subtypes after forebrain ischemia within the striatum is a matter of controversy. As some researchers could not detect Dopamine- and cAMP-regulated phosphoprotein, Mr 32 kDa (DARPP-32), a marker for striatal interneurons, positive cells within newly generated neurons, the same research group show that almost all newly generated neurons are calretinin and Sp8, marker for OB and striatal interneurons, positive (Liu et al., 2009).

Taken everything together, it is clear that some brain regions are able to provide NSCs for injury induced neurogenesis. However, the origin of the newly generated neurons and the specific neuron subtype are still to be investigated.

Mechanisms to activate and increase injury induced neurogenesis are still unclear. The first to achieve a manipulation within these mechanisms were Nakatomi et al. (Nakatomi et al., 2002). They used a cocktail of epidermal growth factor (EGF) and fibroblast growth factor-2 (FGF-2) to boost endogenous hippocampal injury induced neurogenesis after global ischemia. EGF and FGF are potent NSC mitogens.

To further understand the brain repair mechanisms, researchers focused more on the endogenous microenvironment to activate NSCs. Here, immune response and inflammatory signals are thought to be crucial for the activation of stem cells upon brain damage (Nakafuku and Grande, 2013). However, the entire mechanism and signals are to be investigated and understood.

There is strong evidence, that brain repair is also regulated on an epigenetic base. After injury, there are mechanisms to reactivate developmental programs important for

neurogenesis with a higher capability of producing new neurons. This reactivation of repair mechanisms is coupled with the overall demethylation of the DNA (Hirose et al., 2013; Lee et al., 2013).

Previous tagmentation-based whole genome bisulfite sequencing (T-WGBS) data (Wang et al., 2013) from a cooperation with Christoph Plass group, had shown differentially methylated regions (DMRs) within NSCs from bilateral common carotid artery occlusion (BCCAO) mice (unpublished data). 75% of these DMRs are overlapping with the histone mark H3K4me1 which is associated with active enhancers (Buecker and Wysocka, 2012).

The DMRs were compared to the brain region- and developmental stage-specific histone modification ChIP-seq datasets available from ENCODE (Hon et al., 2013) and transcription factor binding sites (TFBS) were mapped. Here, the binding site for the LIM-homeodomain transcription factor *Isl1* was one of the most prominent.

These findings, suggest, that certain developmental transcription factors can bind the DNA upon brain injuries and activate the generation of alternative neuronal subtypes. *Isl1* has been identified as such a transcription factor (unpublished data).

Taken everything together, the methylome changes upon brain injury could provide a promising target to activate injury induced neurogenesis and will be a crucial part of this thesis. However, DMRs are still to be investigated and the effects of transcription factors on the injury methylome are unknown.

1.2 *Isl1*

Isl1 or *Islet-1* is a LIM-homeodomain transcription factor. LIM transcription factors were originally named after the three transcription factors *Lin11*, *Isl1* and *Mec3*, that contain the same domain (Sánchez-García and Rabbits, 1994). Around 100 LIM-proteins are known in humans. All of them contain a two zinc-fingers, that is able to bind 2 zinc ions and to form protein-protein interactions (Michelsen et al., 1993). The LIM domain is cytosine rich and approximately 50-60 amino acids long.

LIM proteins can contain one or multiple LIM domains. Those domains can be associated with homeodomains, kinase, GAP (GTPase activating protein), SH3 or PDZ domains (Hunter and Rhodes, 2005). The LIM protein superfamily is associated with intracellular signaling, cellular structures, transcription factors and transcriptional coactivators.

In humans, 12 LIM-homeodomain proteins are known. They play key roles in developmental transcription regulation. LIM-homeodomain proteins are characterized by their two terminal LIM domains and a central homeodomain to interact with specific DNA elements (Howard and Maurer, 2000).

Isl1 is expressed in a large number of tissues during embryogenesis. It has been found in the central and peripheral nervous system, neural retina, inner ear, pharyngeal mesoderm and endoderm, cardiovascular system, gastrointestinal system and hindlimb (Zhuang et al., 2013). It is associated with cell proliferation, differentiation and survival. Isl1 is expressed in the developing and adult striatum of mice. The expression levels are highly dynamic within different cell types and vary over time. Cholinergic cells for example show a high and continuous Isl1 expression, whereas in non-cholinergic cells, the expression is downregulated during development. This indicated a key function of Isl1 in neuronal differentiation (Wang and Liu, 2001).

Previous studies revealed, that Isl1 has the capability to promote the generation of neurons from postnatal SVZ precursors (Stenman et al., 2003). However, the effects of Isl1 alone were only marginal and no neurogenesis or striatal differentiation could be observed. Thus, the overexpression of Isl1 in the neonatal brain produces new neurons in the striatum, however a striatal projection neuron phenotype could not be observed (Rogelius et al., 2006).

Later studies with a combination of Isl1 and Neurogenin-2 (Ng2) were able to show the SVZ cells can be redirected from their normal migration route to different brain areas (Rogelius et al., 2008). The newly generated cells show a neuroblast like morphology in the striatum.

1.3 Adeno-associated virus

Adeno-associated viruses (AAVs) have first been identified as a side product of Adenovirus (Ad) purification in 1965 (Atchison et al., 1965). Over the last years, it has become a promising candidate not only in the field of biomedical research but also for gene therapy approaches. It is widely used to introduce and study gene expression in mammals in vitro as well as in vivo.

1.3.1 Characteristics of AAVs

Adeno-associated viruses are small viruses without an envelope. They are capable of packing a single stranded DNA genome of approximately 5kb in total length (Wu et al., 2010). It is a member of the family Parvoviridae and the wildtype serotypes have not been associated with any disease affecting mammals (Calcedo et al., 2011). Therefore, it can be used under biosafety level 1 according to Directive 2000/54/EC of the European Parliament.

The virus consists of a T = 1 icosahedral capsid with a diameter of 25nm (**Figure 3a**) and can resist short exposure to acidic pH, heat and proteases (Rayaprolu et al., 2013). AAVs are capable of packing double- and single-stranded DNA. In case of single stranded DNA, positive and negative strands are packed equally well (Zhou et al., 2008). The viral genome contains three open-reading-frames (ORFs), coding for eight proteins under the control of three promoters (**Figure 3b**) (Sonntag et al., 2010).

At either end of the genome, inverted terminal repeats (ITRs) can be found. They are T-shaped, 145 bases long and serve as origin of DNA replication and are required as packaging signal (McLaughlin et al., 1988). ITRs are the only sequences needed for recombinant AAVs (rAAVs). As ITRs do not have promoter or enhancer activity in the absence of the Rep protein, promoter, poly(A) and eventually splicing signals must be included in the rAAV vector.

For the DNA replication, the AAV protein Rep78 or Rep68, the cellular DNA polymerase δ complex, replication factor C, the proliferating cell nuclear antigen and the minichromosome maintenance complex are needed (Ni et al., 1998). AAVs cannot replicate itself. They need a helper virus. Over the last years, Ad, herpesvirus and baculovirus has been used to provide different helper functions in AAV replication (Janik et al., 1981; Slanina et al., 2006; Smith et al., 2009).

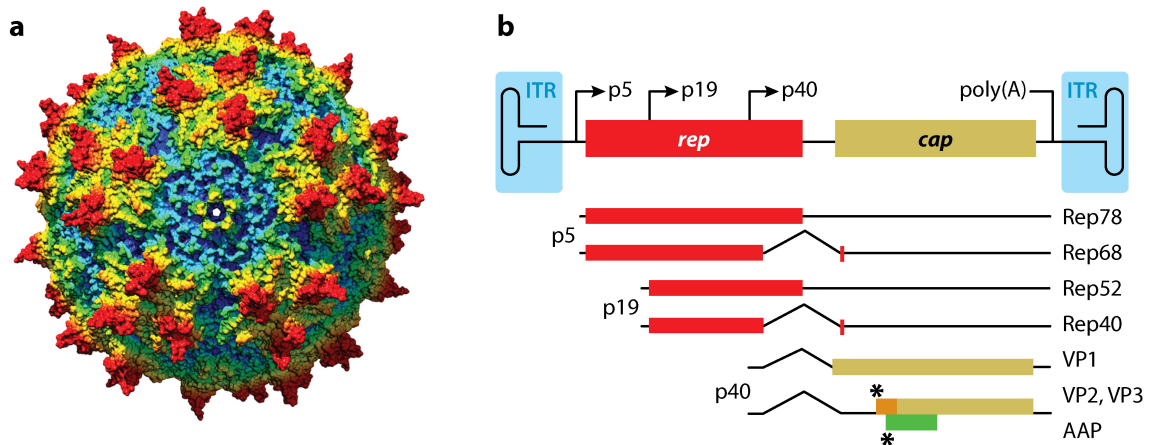


Figure 3 Adeno-associated virus (AAV) structure (a) AAV capsid surface. Shown is a depth-cued space-filling model generated from the crystal structure of AAV2 (Xie et al., 2002). Surface amino acids are colored according to their relative distance from the center of the capsid, in the following order: blue (closest), cyan, green, yellow and red (farthest). **(b) Genetic map of AAVs.** The ~5-kb AAV genome contains three open reading frames (ORFs) that code for functional proteins. The rep ORF (red) codes for four Rep proteins (Rep78, Rep68, Rep52, and Rep40) that are synthesized from mRNAs initiated from the p5 and p19 promoters. The p40 promoter initiates an mRNA that is alternatively spliced to make three capsid proteins from the cap ORF (yellow) and one assembly-activating protein (AAP) (green). Also shown are the 145-base T-shaped AAV inverted terminal repeats (ITRs) (blue). Adapted from (Samulski and Muzyczka, 2014).

1.3.2 Production

In early production methods, Ad was used as a helper virus. However, Ad cannot be removed sufficiently from the rAAV stock. CsCl density centrifugation followed by heat inactivation of Ad was used to produce Ad free rAAVs. A small amount of Ad cannot be removed using this strategy and a high rate of cell toxicity was observed in early rAAVs (Samulski et al., 1989). In 1998 three groups simultaneously achieved to clone the necessary adeno-helper functions on a separate plasmid and eliminate the genes needed for Ad replication (Jagannathan et al., 2012; Matsushita et al., 1998). From now on, coinfection with Ad was not needed anymore. The group of Prof. Grimm furthermore established a double transfection protocol with an alternative mouse mammary tumor virus LTR promoter and eliminated cross contaminations with other serotypes (Grimm et al., 1998).

The most commonly used method to produce AAVs is the triple-plasmid transfection (Grimm et al., 1998). HEK293T cells that express the Ad proteins E1a, and E1b are used as hosts. E1a is a transcriptional activator that induces the p5 AAV promoter and also

induces the S phase in host cells. E1b and the helper functions on a separate plasmid, E2a, E4 and VA RNA perform various tasks in AAV replication (Chang et al., 1989). The cells are then transfected with a plasmid containing the transgene with an appropriate promoter and ITRs, a plasmid carrying the serotype specific rep and cap sequences and a plasmid for the adeno helper functions (**Figure 4**).

Various purification methods have been used over the last years. Affinity chromatography, tangential flow filtration, and serotype specific monoclonal antibody columns have been established. However, those methods are highly serotype specific and for new designed AAVs those methods do not work. To isolate rAAV capsids from empty capsids, only CsCl or iodixanol density centrifugation has been proven to work (Strobel et al., 2015).

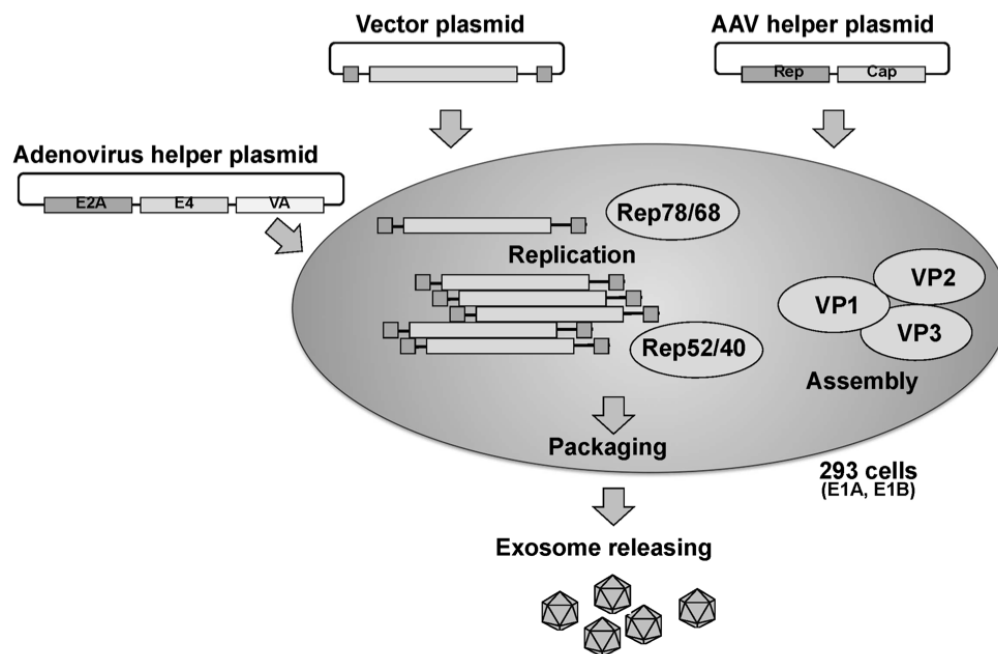


Figure 4 Recombinant Adeno associated virus (AAV) production using the triple-plasmid transfection method. Human embryonic kidney (HEK) cells are transfected with a vector plasmid carrying the transgene, an AAV helper plasmid and a plasmid carrying the appropriate Rep and Cap for the specific serotype. The transfection is followed by replication, assembly and packaging within the HEK cell. The essential proteins are split between the helper plasmid (E2A, E4 and VA) and the HEK cells (E1A and E1B). Adapted from (Okada, 2013).

1.3.3 Designer AAVs

Over the last few years, new AAV serotypes have been generated. These serotypes are more tissue and cell specific than their wildtype counterparts. One way to produce new AAV capsids is a Cre depended selection method (CREATE) (Deverman et al., 2016). Here, cre expressing cells are used as a marker for AAV infection, and a central nervous system (CNS) specific serotype could be isolated. Another approach is to shuffle the AAV wildtype capsids, using the bioinformatics tool SCHEMA (Ojala et al., 2017). With this program, capsid-host interactions are simulated, and 3D structures are analyzed and predictions for tissue and cell specific AAVs are made.

1.4 Aim of the project

This thesis aims the production of an *Isl1* overexpressing AAV that specifically targets NSCs in the V-SVZ to study the cellular and molecular response of NSCs in the ischemia damaged brain.

As previously shown in our lab, the epigenetic landscape of V-SVZ NSCs is changing upon ischemic injury (Bobadilla, 2016). Highly methylated regions become demethylated and accessible for transcription factors, whereas other regions become methylated and less accessible. Within 20% of all hypomethylated regions, the motive for the LIM homeodomain transcription factor *Isl1* is present. *Isl1* has been identified as a potential neurogenesis activator after brain injuries in previous studies (1.2) and will be the focus of this thesis.

We hypothesized that the transcription factor can target the hypo DMRs in V-SVZ NSCs after ischemia and induce side specific migration and differentiation of newly generated neurons. In this process, alternative neuronal subtypes should be identified within the striatum (Figure 5).

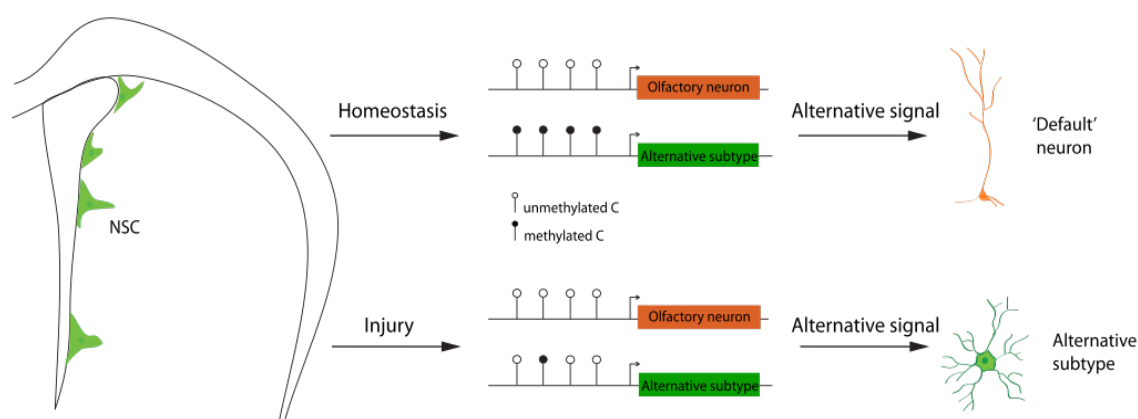


Figure 5 Proposed model for the molecular regulation of injury-induced fate plasticity. Open and filled circles represent unmethylated and methylated CpGs respectively at regulatory elements. In this model, injury signals induce localized demethylation at regulatory regions of neuron subtype-specifying transcription factors that are otherwise silent. Adapted from (Bobadilla, 2016).

2 Material and methods

2.1 Materials

2.1.1 Reagents

Table 1 Chemicals, Kits and Reagents

Reagent	Company
10xHBSS	ThermoFisher
12% Mini-Protean TGX Stainfree Protein gels 12 well 20µl	BioRad
1M HEPES	ThermoFisher
1M MgCl ₂	Sigma-Aldrich
1M TrisHCl pH 7,5	Sigma-Aldrich
2x Sensimix II Probe kit	Bioline
4xLaemmli Sample Buffer	BioRad
Accutase	Sigma-Aldrich
Agencourt Ampure XP beads	Beckman Coulter
B27-supplement	ThermoFisher
Benzonase Nuclease 25 U/µl	Sigma-Aldrich
Betaine 5M	Sigma-Aldrich
Clarity™ Western ECL Substrate, 200 ml	BioRad
CsCl	Sigma-Aldrich
D-Glucose	Sigma-Aldrich
DMEM, high glucose, no glutamine	Life Technologies
DPBS without Ca and Mg	PAN-Biotech
DTT 100mM	Invitrogen
EtOH	Sigma-Aldrich
Falcon™ Cell Strainers	ThermoFisher
FBS	Biochrom

Reagent	Company
FGF	Pellobiotech
Fluoromount-G	eBioscience
Gentle MACS C-Tubes	Miltenyi Biotec
HBSS	ThermoFisher
hEGF	PromoKine
Heparin	Sigma-Aldrich
Histofix 4% PFA	Roth
Hourse Serum	Biochrom
Isofluran	Zoetis
Isopropanol	Sigma-Aldrich
2xHiFi HotStart ReadyMix	KAPA Biosystems
Ketavet	Pfizer
L-Glutamine	Life technologies
NP-40	Sigma-Aldrich
Neural Tissue Dissociation Kit (T)	MACS Miltenyi Biotec
PureLink™ HiPure Plasmid Filter Maxiprep Kit	ThermoFisher
PureLink™ HiPure Expi Plasmid Megaprep Kit	ThermoFisher
Mercaptoethanol	Sigma-Aldrich
Metamizol	Dr Ehrenstorfer GmbH
Na ₂ HPO ₄ · 7H ₂ O	Sigma-Aldrich
NaCl	Sigma-Aldrich
NaH ₂ PO ₄	Santa Cruz
NaOH	Fluka
Neurobasal medium A	ThermoFisher
Non-Fat Dry Milk	Roth
Nuclease free water	Ambion
PAGE Ruler Prestained Protein Ladder	Life technologies

Reagent	Company
PEG	AppliChem
PEI	Sigma-Aldrich
Pen/Strep	ThermoFisher
Pierce™ BCA Protein Assay Kit	ThermoFisher
PicoPure™ RNA Isolation Kit	ThermoFisher
2x Power SYBR™ Green PCR Master Mix	Life Technologies
Proteinase inhibitor	Sigma-Aldrich
QIAprep Spin Miniprep Kit	Qiagen
Qubit™ dsDNA HS Assay Kit	Life technologies
Rampun	Bayer
RNase inhibitor	TaKaRa
SDS	Serva
Slide-A-Lyzer™ G2 Dialysis Cassettes, 20K MWCO, 15 mL	ThermoFisher
Sodium Azide	Acros Organics
Sodium phosphate dibasic heptahydrate	Sigma-Aldrich
Sodium phosphate monobasic	Sigma-Aldrich
SuperScript II first strand buffer	Invitrogen
SuperScript II reverse Transcriptase	Life technologies
Surfact-Amps NP40	ThermoFisher
Trans-Blot® Turbo™ RTA Midi Nitrocellulose Transfer Kit	BioRad
Trisbase	Acros organics
Triton X-100	Sigma-Aldrich
Trypsin	Invitrogen
Trypton/Pepton	Fluka
Tween 20	Sigma-Aldrich
Yeast Extract	GERBU

2.1.2 Buffers and media

PBS (20x)

NaCl	160g/l
KCl	4g/l
KH ₂ PO ₄	4.8g/l
Na ₂ HPO ₄ ·7H ₂ O	35.6g/l

The pH is adjusted to 7.4 with 0.1M HCl. The solution is brought to a final volume of 1l with dH₂O.

TBS (10x)

Trisbase	24.2g/l
NaCl	80g/l

Mix in 800 ml ultra-pure water, adjust pH to 7.4 with pure HCl and fill up to 1 litre.

0.2M Monobasic Stock

NaH ₂ PO ₄	27.8g/l
----------------------------------	---------

0.2M Dibasic Stock

Na ₂ HPO ₄ ·7H ₂ O	53.65g/l
---	----------

0.1M Phosphate buffer

Combine 57ml of the monobasic stock with 243ml of the dibasic stock and bring volume up to 600ml to obtain a 0.1M Phosphate buffer with a pH of 7.4.

TBS++

TBS	100ml
Horse serum	3ml
Triton X-100	0.25ml

Perfusion Solution

Ketavet (1:5)	4ml
Rompun	2ml
NaCl 0.9% sterile	8ml

Dissection solution

HBSS (10x)	50ml
HEPES (1M)	1.25ml
D-glucose	3.25g
Pen/Strep	5ml

FACS-buffer

dPBS	450ml
FCS	50ml

NBM Medium

Neurobasal medium A	500ml
L-Glutamine	5ml
B27-supplement	10ml
Pen/Strep	5ml
Heparin	500 μ l
hEGF	20 μ l
FGF	20 μ l

Growth-factor free NBM Medium

Neurobasal medium A	500ml
L-Glutamine	5ml
B27-supplement	10ml

Benzonase buffer

TrisHCl	50mM
MgCl ₂	2mM
NaCl	150mM
Adjust pH to 8.5	

Na-HEPES resuspension buffer

HEPES	50mM
NaCl	150mM
EDTA	25mM

CsCl topping solution

CsCl	550g/l
------	--------

Prepare in Na-HEPES resuspension buffer and adjust refractive index to 1.3710 at room temperature

40% PEG8000 solution

PEG	40% v/v
NaCl	1.915M

DMEM Medium

FCS	10%
Pen/Strep	1%
L-Glutamine	1%

Add to DMEM high glucose, no glutamine

TBS-T

TBS	1x
Tween20	0.05%

10x Running Buffer

Glycin	144g/l
TrisBase	30g/l
SDS	1%

Stripping Buffer

Glycin	1M
pH 1.8	

NP-40 Lysis Buffer

NP-40	1%
NaCl	150mM
Tris	50mM
Proteinase inhibitor	1x
SDS	0.1%
β -Mercaptoethanol	10mM

2.1.3 Antibodies**Table 2 Antibodies for IHC, Western Blots and FACS**

Antibody	Company	Dilution
IHC		
DAPI	Sigma-Aldrich	1:4000
dk anti ck 647	Jackson Immuno Research	1:400
dk anti gb 405	Sigma-Aldrich	1:400
dk anti gt 546	Life technologies	1:400
dk anti ms 488	Invitrogen	1:400
dk anti rat 405	Abcam	1:400
dk anti rb 405	Abcam	1:400
dk anti rb 488	Invitrogen	1:400

dk anti rb 647	Life technologies	1:400
ck anti GFAP	GeneTex	1:1000
gb anti DCX	Merck	1:500
gt anti mCherry	SICCGEN	1:500
ms anti GFAP	Millipore	1:2000
ms anti SOX2	Abcam	1:100
rat anti DARPP_32	R&D Systems	1:200
rb anti Isl1 IHC	Abcam	1:300
rb anti S100beta	Abcam	1:100
ms anti NeuN	Millipore	1:300
WB		
rb anti Isl1 WB	Abcam	1:10000
rb anti β -Actin	Cell Signaling Technology	1:1000
rb anti Histon 3	Cell Signaling Technology	1:1000
gt anti rb HRP	Dianova	1:5000
FACS		
Ter119 APC-Cy7	Biolegend	1:100
O4 APC-Cy7	MACS	1:50
CD45 APC-Cy7	BD Bioscience	1:200
GLAST APC	MACS	1:20
CD9-FITC	eBioscience	1:300
Cytox Blue dead cell stain	Invitrogen	1 μ M

2.1.4 Primer

Table 3 Primer for AAV Titration, Expression qPCR and reverse transcription

Primer name	Sequence
Cre qPCR AAV Titer FW	ACTGACGGTGGGAGAATGTT
Cre qPCR AAV Titer RV	CCAGGCTAAGTGCCTTCTCT
Cre qPCR AAV Titer Probe	FAM-ACCTGCGGTGCTAACCAGCGT-BHQ1
GAPDH qPCR FW	CTCCTGCACCACCAACTGCT
GAPDH qPCR RV	GGGCCATCCACAGTCTTCTG
IS PCR primers	AAGCAGTGGTATCAACGCAGAGT
Isl1 qPCR FW	CTGCAAATGGCAGCCGAA
Isl1 qPCR RV	GCTTCTCGTTGAGCACAGTC
oligo dT	AAGCAGTGGTATCAACGCAGAGTACT30VN
TSO-Biotin	Biotin- AAGCAGTGGTATCAACGCAGAGTACATrGrG{G}

2.2 Methods

2.2.1 Adeno Associated virus

2.2.1.1 Production

For the AAV production, HEK293T (Human Embryonic Kidney) cells from ATCC were used. For harvesting and reseeding cells, they were washed with 10ml dPBS and dissociated using 5ml of 0.25% Trypsin per flask. After counting, 4.5×10^6 cells were reseeded to 150cm² dishes in 22ml DMEM medium and incubated for 2 days at 37°C and 5% CO₂. A total of 300 plates were prepared this was to obtain an appropriate virus titer.

After two days, cells were transfected using 2mg/ml Polyethylenimine and the triple transfection method previously described (Grimm et al., 1998). The final transfection reagent included 14.67µg of Adeno helper plasmid, AAV1_P5 capsid plasmid and CMV_Is11_P2a_Cre plasmid, 150mM NaCl, 56.85µl PEI and the volume was adjusted to 3.2ml per plate. The solution was added dropwise to the confluent plates containing the HEK293T cells.

Three days after the transfection, cells were harvested by scraping, 30 plates were processed per 50ml falcon. Pellets were resuspended in 15ml Benzonase buffer. Cells were disrupted by 5 freeze-thaw cycles using liquid nitrogen and a 37°C water bath. Afterwards, samples were sonicated for 1min20s and 75U/ml Benzonase was added. Samples were incubated at 37°C for 1h and inverted every 10min followed by 15min centrifugation at 4000g. Supernatant was collected, 1/39th volume 1M Calcium chloride added and samples were incubated 1h on ice followed by 15min centrifugation at 4°C and 10000g. 1/4th volume 40%PEG8000/1.915M NaCl was added to supernatant and incubated 3 hours on ice. Samples were centrifuged 30min at 2500g at 4°C and pellet was resuspended in 10ml Na-Hepes resuspension buffer. Pellet was stored on a roller at 4°C overnight to resuspend the pellet completely.

Samples were then centrifuged at 2500g, 4°C for 30min and supernatant was filled up to 24ml with Na-Hepes resuspension buffer. 13.2g Cesium chloride was added and RI was adjusted to 1.3710. Samples were transferred to ultracentrifugation tubes and filled up with topping solution without bubble formation. Tubes were centrifuged in a 70TI rotor for 22h at 45000RPM at 21°C.

After ultracentrifugation, fractions with a RI between 1.3711 and 1.3766 were collected and combined, followed by dialysis in G2 Dialysis Cassettes in PBS. Ice-cold PBS was exchanged after 30min, 1h, 2h, overnight, 2h and 2h. The dialyzed AAV solution was concentrated using Amnicon-Ultra-15 columns as described in the manufacturers protocol. The final AAV solution was aliquoted and stored at -80°C.

2.2.1.2 Titer

The titer of the AAV1_P5_CMV_Is11_P2A_Cre was measured by quantitative Real Time PCR (qRT-PCR). 10µl of AAV solution was mixed with 10µl of DNase free water and lysed with 20µl of 2M NaOH for 30min at 56°C. The solution was neutralized with 38µl 1M HCl and filled up to 1ml with H₂O. The same procedure was done with H₂O and purified CMV_Is11_P2A_Cre plasmid instead of AAV as a negative and positive control. For the titration, standards from 1.75×10^2 - 1.75×10^9 DNA molecules were made with the purified plasmid.

For the qPCR, reagents were mixed as shown in **Table 4**. The cycling conditions contained a 10min initial denaturation step at 95°C followed by 40 cycles of 10s denaturation at 95°C and 60°C combined annealing and extension for 20s. Samples were analyzed in triplicates and the calculated concentration for the AAV1_P5 with the CMV_Is11_P2A_Cre was 8.89×10^{11} viral genomes (vg)/ml.

Table 4 qPCR setup for AAV titration

Reagent	Volume for triplicates (µl)	Final concentration
2x Sensimix II Probe kit	17.5	1x
Cre qPCR AAV Titer FW Primer	1.4	0.4µM
Cre qPCR AAV Titer RV Primer	1.4	0.4µM
Cre qPCR AAV Titer Probe	0.35	0.1µM
DNase free water	9.35	
Alkaline lysis/Standard	5	

2.2.1.3 *In vivo* quantification

To quantify the infected cell populations, 10^9 vg of the AAV1_P5_CMV_Is11_P2A_Cre virus were injected into the ventricle of 8-week-old male TdTom-flox mice. 5 days after injection mice were perfused, brains were dissected and processed in coronal sections. Brain slices were stained with the primary antibodies $rb\alpha$ S100beta, $gb\alpha$ DCX, $gt\alpha$ mCherry, $ms\alpha$ SOX2 and $ck\alpha$ GFAP as described in 2.2.3.5. The secondary Antibodies $dk\alpha$ rb 405, $dk\alpha$ gb 405, $dk\alpha$ ms 488, $dk\alpha$ gt 546 and $dk\alpha$ ck 647 were used. Images were taken on a Leica TCS SP5 confocal microscope. Quantification was done by using ImageJ.

2.2.2 *In vitro* experiments

2.2.2.1 *NSC isolation and cultivation*

For the isolation of NSCs, mice were sacrificed by cervical dislocation and isolated brains were placed in dissection solution on ice. The subventricular zone was microdissected as wholemount as previously described (Mirzadeh et al., 2010). The cerebellum was removed close behind the triangle cranial and hemispheres were separated by cutting. A caudal incision where the hippocampus connects to the cortex was made and the hippocampus was pulled away to uncover the lateral wall of the ventricle. The SVZ is isolated by three cuts, one dorsal, one ventral and one parallel to the lateral wall followed by cutting around 200 μ m underneath the structure.

Stem cells are isolated using the Neural Tissue Dissociation Kit T. The digest is stopped by adding 5ml of NBM medium and cells are isolated by passing the digested tissue through a 40 μ m cell strainer. After washing the cells twice, they are transferred to a 25cm² cell culture flask in 7ml NBM medium. After reaching confluency, spheres were dissociated using Accutase and transferred first to a 75cm² flask and later to 150cm² flasks. Cells were split 1:10 two to three times per week. Cells were grown at 37°C and 5% CO₂. NSCs for *in vitro* tests were a maximum of 6 weeks in culture.

2.2.2.2 RNA isolation

For the RNA isolation, the PicoPure™ RNA Isolation Kit was used. 10^4 cells from the according time point were resuspended in 100µl extraction buffer and RNA isolation was performed according to the manufacturers protocol including a DNA digestion step with 5µl DNase. RNA was resuspended in 11µl Nuclease free water.

2.2.2.3 Reverse transcription

The reverse transcription (RT) was performed as previously described (Picelli et al., 2014). 2.3µl of the isolated RNA was mixed with 1µl of 10µM oligo-dT primer and 1µl of 100µM dNTPs and incubated for 3min at 72°C. The final RT mix was set up according to **Table 5**. 5.7µl of RT mix were mixed with 4.3µl of RNA mix. The cycling conditions were according to **Table 6**. After the RT, DNA was amplified using the KAPA HiFi HotStart ReadyMix and IS PCR primers(10µM) and cycling conditions according to **Table 7**. cDNA was cleaned up using Ampure XP beads and the manufacturers protocol. cDNA concentration was measured using the Qubit™ dsDNA HS Assay Kit And 2ng cDNA were used for the following qPCR.

Table 5 Reverse transcription mix

Component	Volume (µl)	Final concentration
SuperScriptII reverse transcriptase (200U/µl)	0.50	100U
RNAse inhibitor (40U/µl)	0.25	10U
Superscript II first-strand buffer (5x)	2.00	1x
DTT (100mM)	0.06	5mM
Betaine (5M)	0.06	1M
MgCl ₂ (1M)	0.10	6mM
TSO (100µM)	0.29	1µM
Nuclease-free water	0.29	
Total volume	5.70	

Table 6 Cycling conditions for reverse transcription

Cycle	Temperature (°C)	Time (min)	Purpose
1	42	90	RT and template switching
2-11	50	2	Unfolding of RNA secondary structures
	42	2	Completion of RT and template switching
13	70	15	Enzyme inactivation
13	4	hold	Safe storage

Table 7 Cycling conditions for DNA amplification

Cycle	Denature	Anneal	Extend	Hold
1	98°C/3min			
2-14	98°C/20s	67°C/15s	72°C/6min	
15			72°C/5min	
16				4°C

2.2.2.4 qPCR

qRT-PCR was performed using the Power SYBR Green Master Mix and the primer pairs GAPDH qPCR FW, GAPDH qPCR RV and Is11 qPCR FW, Is11 qPCR RV. 2ng of cDNA was mixed with 0.5 µl of Primers (5µM) and 5.5µl Power SYBR Green Master Mix. Samples were adjusted to a total volume of 10µl. Samples were analysed in triplicates in a 384 well plat with a CFX96 TouchTm Real-Time PCR detection System with an initial denaturation step at 95°C for 10min followed by 45 cycles of 15s at 95°C and 30s at 55°C.

For the analysis, the fold change in expression levels were calculated as in Equation 1.

$$\bar{x}(C_T^{Isl1}) - \bar{x}(C_T^{GAPDH}) = \Delta C_T$$

$$\Delta C_T^{infected} - \Delta C_T^{control} = \Delta\Delta C_T$$

$$fold\ change = 2^{-\Delta\Delta C_T}$$

Equation 1 Calculation of fold change in expression levels

2.2.2.5 Western Blots

For Protein analysis, cells of the according time point were harvested and lysed in 50-100µl NP40 buffer, according to the pellet size. Cells were lysed for 10min on ice and centrifuged for 5min at 4°C with 13000rpm. The supernatant was collected and used in the Pierce™ BCA Protein Assay Kit. The remaining sample was diluted 1:4 in 4xLaemmli Sample Buffer.

Samples were loaded on 12% Mini-Protean TGX Steinfree Protein gels and run for 15min at 80V in Running Buffer. After 15 min. the voltage was increased to 160V and gel was run until the front reached the bottom of the gel. Gels were blotted using the Trans-Blot® Turbo™ RTA Midi Nitrocellulose Transfer Kit and the Trans-Blot® Turbo™ Transfer System. After blotting, cells were blocked in TBS-T containing 5% NFDM for 2 hours. Membranes were incubated in primary antibodies over night at 4°C followed by 3 washing steps 5min each. Membranes were incubated with Secondary Antibodies for 1 hour at RT followed by 3 washing steps. Bands were visualized using Clarity™ Western ECL Substrate and a ChemiDoc™ Touch Gel Imaging System.

2.2.3 In vivo experiments

2.2.3.1 Mice

Eight week old males from the following mouse strains were used for all experiments, C57BL/6N (wild-type), B6.Cg-Tg(Thy1-Brainbow1.0)HLich (Brainbow) and B6-Gt(ROSA)26Sortm14(CAG-tdTomato)Hze (TdTom-flox). Mice of the same experiment were caged together with water and food ad libitum. A constant 12h light and dark cycle was maintained with a temperature of 22°C. All animal experiments were performed in

accordance with the institutional guidelines of the DKFZ and were approved by the Regierungspräsidium, Karlsruhe.

2.2.3.2 Stereotactic injections

For stereotactic injections, mice were anesthetized using an initial concentration of 3% Isofluran, eyes were protected using Bepanthen crème. 100µl of Metamizol was used as analgesia. The mouse was fixed to a motorized stereotactic frame and Isofluran was kept at a constant rate of 1.5-2%. An approximately 1cm sagittal incision was made along the midline to expose the skull. The instrument was normalized to the Bregma and for injections into the left lateral ventricle a small hole was drilled into the skull using a 25G needle at the coordinates -0.5/-1.1/2.4, for injections into the upper layers of the striatum the hole was drilled at 1/2/2.5 and 0/2/2.3. The solutions were then injected using a 10µl Nanofil syringe with a 33G needle at a constant flow rate of 0.3µl/min. Before removing the needle, an additional 10min elapsed to prevent backflow of the injected solution.

2.2.3.3 Ischemia

Global forebrain ischemia was performed using the BCCAO model as previously described (Speetzen et al., 2013). Mice were anesthetized using 3% Isofluran until the pedal reflex disappeared and eyes were protected using Bepanthen crème. 100-200µl Metamizol was injected as a painkiller depending on the size of the mouse and it was fixed ventral to a prewarmed heat mat and Isofluran was reduced to 2%. An about 1cm sagittal incision between the right eye and ear was made after disinfection of the area and the skin underneath was removed using forceps. A probe holder was fixed to the lateral muscle close to the sculpt using medical glue. The mouse is then turned around and a mouse pillow is used to stretch the neck. After disinfection, a 1.5-2cm incision at the midline was made to expose the trachea. From now on, the fat tissue is opened using forceps until the trachea becomes visible. On each side of the trachea a carotid artery and the vagus nerve appears. The carotis can be distinguished from the vena because its brighter and pulsing. The tissue between carotis and trachea is removed by carefully opening and closing the forceps in this area. When the carotis is free from the surrounding nerve, it can be lifted and a small piece of silk is pulled underneath. When both sides are prepared, the mouse is turned on its side and a Laser Doppler Perfusion Monitoring probe (Laser Doppler Perfusion Monitor PeriFlux System 5010, Perimed) is inserted into the

probe holder. The mouse is turned back to dorsal and warmed using a red-light bulb if necessary. When temperature is around 36.8°C, the carotid arteries are clamped. The regional cerebral blood flow is noted 1min after occlusion and has to be below 13% of the initial value before clamping. If the value is higher, the procedure is terminated, the mouse is stitched and used as a negative control (Sham mouse). If the value drops below 13%, the occlusion is kept for 22min and afterwards the mouse is stitched and after being awake caged with other mice of the same experiment.

2.2.3.4 Perfusion

Mice were sacrificed with an i.p. injection of 800µl perfusion solution followed by a left ventricular perfusion with 15ml of 1xHBSS (Hank's Balanced Salt Solution) to clear blood vessels. The brain tissue was fixed by perfusion with 7ml 4% PFA. After perfusion, the head was cut off followed by skin removal above the skull. Three incisions, medial, left and right lateral at the rostral end of the head were made. The skull was opened by inserting a pointed tip scissor at the Bregma, if Olfactory Bulbs were not needed, or about 1cm caudal of the Bregma if OBs were needed. The Brain was transferred to a 15ml Falcon with 4%PFA and fixed overnight.

2.2.3.5 Immunohistochemistry

After fixation in PFA overnight, Brains were cut on a Leica VT1200 S - fully automated vibrating blade microtome into 50 or 70µm sections. For cutting the OBs, they were embedded into 2% Agarose in TBS. If sections are to be stored long-term, they are placed in TBS containing 0.01% Azide. Sections were rinsed in TBS 4 times, 10min each followed by blocking in TBS++ for at least 60min. After blocking, the sections were incubated with the primary antibodies in TBS++ overnight at 4°C. The next day, sections were again rinsed in TBS 4 times, 10min each, blocked in TBS++ for 30min and incubated with the secondary antibodies in TBS++ for at least 2 hours at room temperature. After incubation with the secondary Antibodies the sections were rinsed 4 times 10min in TBS and mounted to cover slips using Fluoromount G and visualized under the microscope.

2.2.3.6 Fluorescence-activated cell sorting

Cells were isolated as described in 2.2.2.1. and washed in twice FACS buffer to stop the digest and finally resuspended in 95µl PBS plus 5µl blocking solution per mouse. Control tubes with 20µl for each antibody were prepared and incubated with according antibodies for 20min on ice. Pallet was washed twice in FACS buffer to remove unbound antibodies and finally resuspended in 150µl FACS for controls and 200µl/mouse for samples. Cells were sorted with a BD FACSAria III into 500µl Growth-factor free NBM Medium. As a negative control, a section of the cortex was prepared the same way and sorted.

3 Results

3.1 Transplantation

As previously shown in our lab, the epigenetic landscape of V-SVZ NSCs is changing upon ischemic injury (Bobadilla, 2016). Therefore, we were investigating the effect of overexpressing *Isl1*, a transcription factor whose transcription factor binding site is present in 20% of hypomethylated enhancer regions (Bobadilla 2016). Therefore, we generated an AAV based overexpression construct.

The construct is based on an *Isl1* overexpressing AAV vector (**Figure 6b**) combined with a tdTomato reporter mouse (**Figure 6a**). Upon successful infection and expression of the viral *Isl1* and the Cre recombinase the loxP flanked stop codon of the TdTomato-flox reporter mouse is cut out and *Isl1* overexpressing cells as well as their progeny remain TdTom positive.

For all of the following experiments, a newly screened AAV serotype with a high tropism for NSCs was used. The AAV was screened in cooperation with the lab of Prof. Grimm (unpublished data). To further analyze the dynamics and infection efficiency of this newly generated serotype called AAV1_P5, several experiments were performed in vitro prior to the actual transplantation approach.

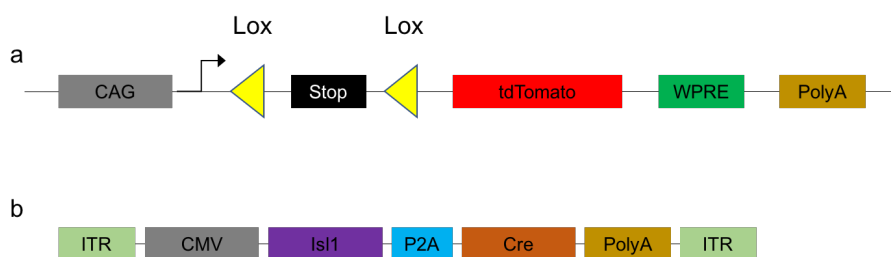


Figure 6 Genetic background of the reporter system (a) Reporter cassette of TdTom flox mice.

The tdTomato fluorescent gene (red) is downstream of a loxP flanked (yellow) stop codon (black). Upon Cre recombinase activity, the stop codon is removed and tdTomato is expressed under the CAG promoter (gray). WPRE., woodchuck hepatitis virus post-transcriptional regulatory element. **(b) *Isl1* overexpressing AAV cassette.** The *Isl1* gene (purple) is under the regulation of a CMV promoter (gray) and followed by a P2A cleavage site (blue). To activate the reporter system, a cre recombinase (orange) is added followed by a PolyA signal (dark yellow). The construct is flanked by inverted terminal repeats (green).

3.1.1 Infection efficiency in vitro

To test the infection efficiency of the AAV1_P5-CMV_Isl1_P2A_Cre construct in vitro, freshly isolated TdTom-flox NSCs were transduced with a MOI of 10^4 . Cells were cultured in NBM medium and were microscopically analyzed after 24h, 48h, 72h and 5 days.

Already after 24 hours, almost all cells were TdTomato positive (**Figure 7a**). The virus was kept in the media and 48 hours Figure 7b and 5 days (data not shown) post infection almost all newly formed spheres showed a bright TdTomato signal (**Figure 7b**).

After 48h the infected cells showed a slight inhibition in growth compared to the control. However, this effect was not detectable 5 days post transduction.

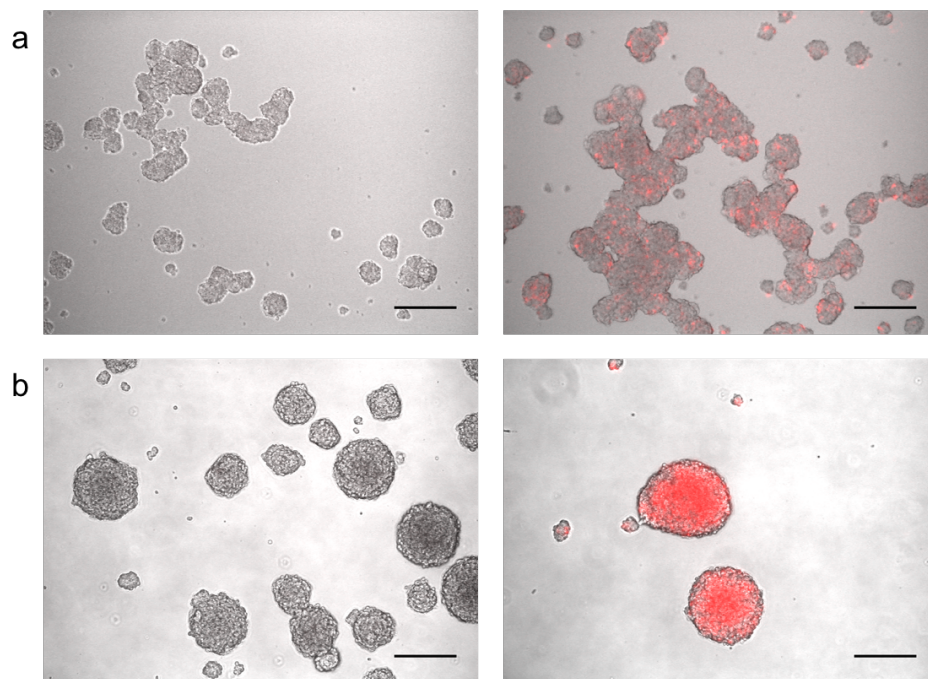


Figure 7 Infection efficiency assay in vitro. TdTom flox NSCs were infected with the AAV1_P5 carrying the Isl1 overexpressing cassette with a Cre recombinase to induce the TdTomato reporter cassette. (a) infection rate after 24h (b) after 48h; left, negative control; right, virus infected

3.1.2 Isl1 Expression

To understand the dynamics of Isl1 expression, the transcription rate upon viral infection was measured after 24h, 72h, 5 days, 7 days and 10 days using a qPCR approach. Different from the tdTomato reporter system, that is constitutively active upon activation due to the recombination in the genome, viral Isl1 expression is expected to vary over time, as AAVs do not integrate into the genome.

For the qPCR, TdTom-flox NSCs were infected with a MOI of 10^4 , mRNA of 10^4 cells was isolated, and reverse transcribed to cDNA. To see the changes in Isl1 transcription, the fold change in mRNA was calculated and samples were normalized to GAPDH and non-infected TdTom-flox NSCs. Samples were measured in triplicates.

The data showed that Isl1 transcription is initiated already 24h after infection (

Figure 8a). After 3 days, a peak of more than the 7000-fold mRNA levels of Isl1 compared to non-infected cells was measured. 5 days post infection, the peak drops and after 10 days, the expression decreased to 20-fold.

This indicates a rapid start of Isl1 transcription in NSCs. However, the transcription and mRNA level drops drastically after only 5 days. To further investigate the expression and translation rates of Isl1 *in vitro*, Western blots were performed for the same time points (

Figure 8b).

The Western Blot indicates a different expression profile to the qPCR. Although the loading was uneven, one could estimate a slight increase in expression of Isl1 over 7 days.

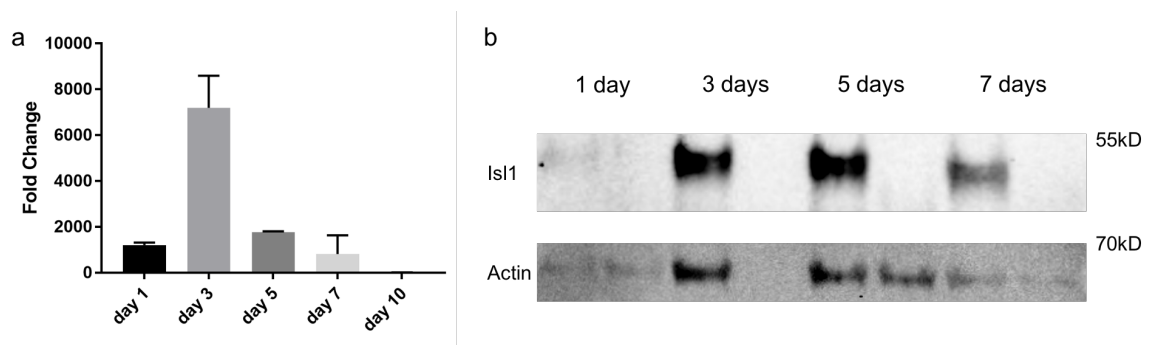


Figure 8 (previous page) Isl1 transcription and expression levels (a) Isl1 transcription levels. qPCR analysis of Isl1 expression of in vitro infected NSCs over a timeperiod of 10 days. Virus was kept in the media for the whole time. **(b) Isl1 expression levels.** Westernblot analysis of isl1 expression. Cell lysate of infected or non infected TdTom flox NSCs were run on a 10% gel under non-denaturing conditions. Lane 1: MW marker, lane 2/3: infected and non-infected after 1 day, lane 3/4: 3 days, lane 5/6: 5 days, lane 6/8: after 7 days.

3.1.3 Transplantation of Isl1 infected cells

To study whether an Isl1 overexpression in injury induced NSCs affects the trajectory of the generated daughter cells towards the injured striatum, NSCs were transduced with an Isl1 overexpressing construct and were re-transplanted to the dorsal area of the striatum.

For this approach, Brainbow mice with an endogenous RFP signal in combination with an AAV9_wt_CAG_Isl1_IRES_DsRed construct were used.

Ischemic injuries were performed and two days later NSCs were isolated by FACS sorting, were infected and re-transplanted to the striatum of wt mice (**Figure 9**). Five weeks post transplantation, mice were perfused and brains were analyzed by IHC and microscopy.

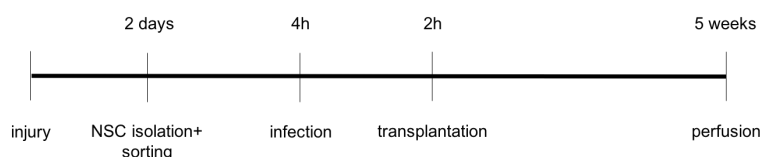


Figure 9 Scheme of the transplantation experimental design. NSCs were isolated, sorted, infected and retransplanted to recipient mice 2 days after BCCAO. Mice were sacrificed for IHC 5 weeks after the surgery.

The FACS strategy was developed according to (Llorens-Bobadilla et al., 2015). In the first round (**Figure 10a**), cells are sorted according to their size and granularity. The second round (**Figure 10b**) excludes doublets. In the third plot (**Figure 10c**), all APC-Cy7 positive cells are excluded. The fluorophore is coupled to antibodies specific for oligodendrocytes (O4 surface marker), erythrocytes (Ter119) and microglia (CD45). Furthermore, dead cells are excluded by SYTOX-Blue staining.

The fourth round (**Figure 10d**) is used to separate neuroblasts and progenitors from NSCs and astrocytes. This is done by sorting for GLAST-APC high cells. In the fifth round (**Figure 10e**), CD9-FITC high cells are sorted. These cells represent the NSC population of the SVZ. To get a clear cut-off between NSCs and Astrocytes, a sample from the cortex is used as NSC-free negative control.

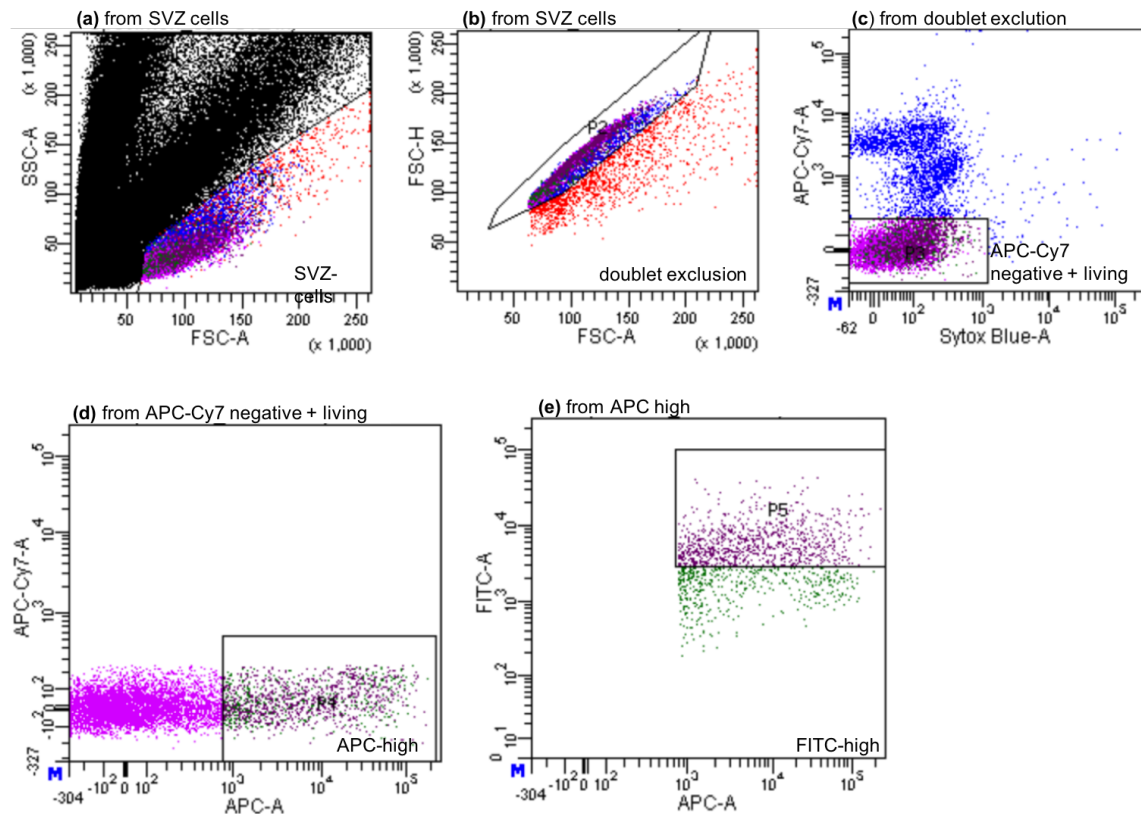


Figure 10 FACS sorting strategie for NSCs from the V-SVZ. The first gate **(a)** uses stringent FSC/SSC gating to exclude myelin particles and cellular debris. The second gate **(b)** excludes cell aggregates. The third gate **(c)** excludes dead and APC-Cy7 positive cells (oligodendrocytes (O4), erythrocytes (Ter119) and mycroglia (CD45)). The fourth gate **(d)** excludes APC (GLAST) low cells (neuroblasts and progenitors). The fifth gates **(e)** separates astrocytes from NSCs by using CD9 as a marker.

After sorting, cells were infected with the AAV9 construct for 2 hours on ice and immediately transplanted into wt recipient mice.

50 μ m brain sections were stained for DARPP-32, a target for dopamine and protein kinase A in the striatum (Svenningsson et al., 2004) and therefore a marker specific for striatal projection neurons. To identify astrocytes and NSCs the glial fibrillary acidic

protein (GFAP) was used as a marker to keep track of the transplanted cells, the sections were further stained for TdTom and Isl1.

Cells were transplanted to the correct position, slightly dorsal to the striatum (**Figure 11a**). The strong TdTom signal and the cell morphology indicated that the cells are still alive and did not die during the whole experimental procedure (**Figure 11b**). After 5 weeks, no Isl1 expression was observed in the transplanted cells.

No cells migrated into the striatum and it was not possible to clarify the final cell identity with the used markers.

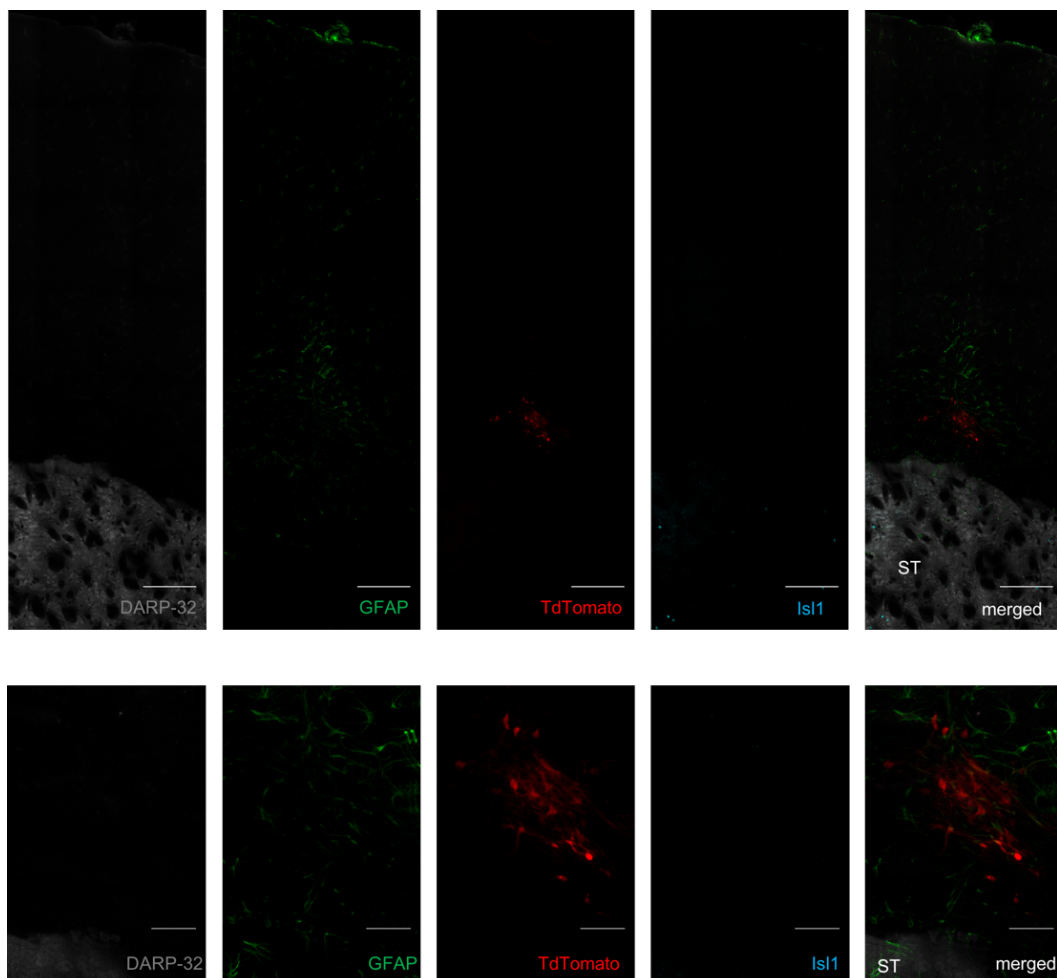


Figure 11 Confocal images of Isl1 infected NSCs 5 weeks after transplantation Sections were immuno stained for DARP-32 (gray), GFAP (green), TdTomato (red) and Isl1 (cyan). Immunostainings were performed 5 weeks after transplantation. **(a)** Overview of transplantation site. ST., Striatum; scale 200nm. **(b)** Close-up of living transplanted cells; scale 50nm

3.2 Direct injection

As a second method to overexpress *Isl1* in NSCs, the viral genomes were injected directly into the ventricle, followed by an ischemic injury after 5 days. The mice were immunohistochemically analyzed 5 weeks after the injury (**Figure 12**).

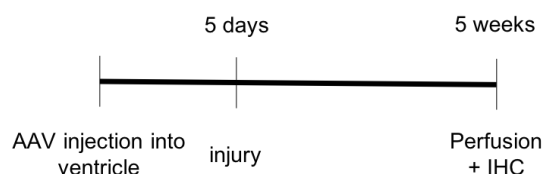


Figure 12 Scheme of the direct injection experimental design. AAV1_P5 with the *Isl1* overexpressing cassette was injected followed by BCCAO 5 days afterwards. Mice were sacrificed for IHC 5 weeks after the surgery.

3.2.1 Infection efficiency in vivo

The AAV1_P5 virus harboring the CMV_*Isl1*_P2A_Cre construct has so far only been tested in vitro. To characterize the construct in-vivo, 5×10^9 vg were injected into the left ventricle of 8-week-old, male TdTom-flox mice

The mice were sacrificed 5 days post injection and the brains were stained for S100 β , DCX, SOX2, TdTom and GFAP.

S100 β is a specific marker for ependymal cells and glial like cells (Beckervordersandforth et al., 2017) and Doublecortin (DCX) is used as marker for immature neurons such as Neuroblasts (Brown et al., 2003) SOX 2 is used as a nuclear marker. It is highly expressed in NSCs but also in ependymal cells and astrocytes (Ellis et al., 2004). GFAP is used as a marker for astrocytes and NSCs (Benner et al., 2013).

To distinguish the different cell types, images were taken on a Leica TCS SP5 confocal microscope and were quantified manually according to **Table 8**, using ImageJ.

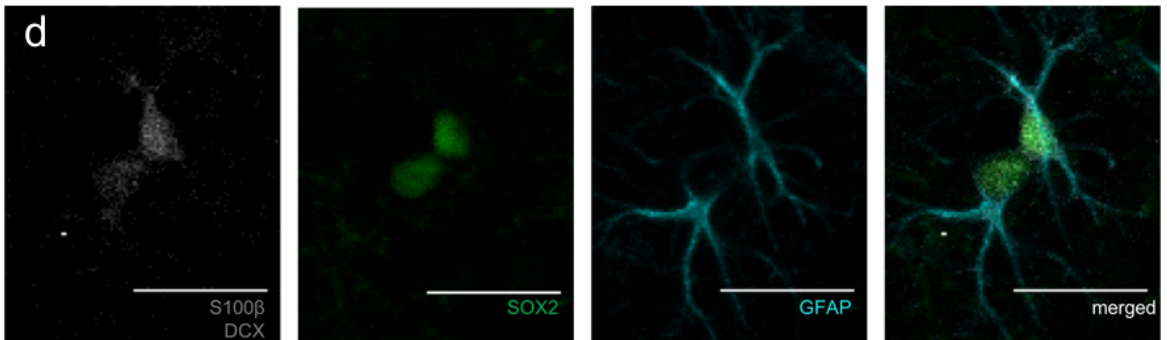
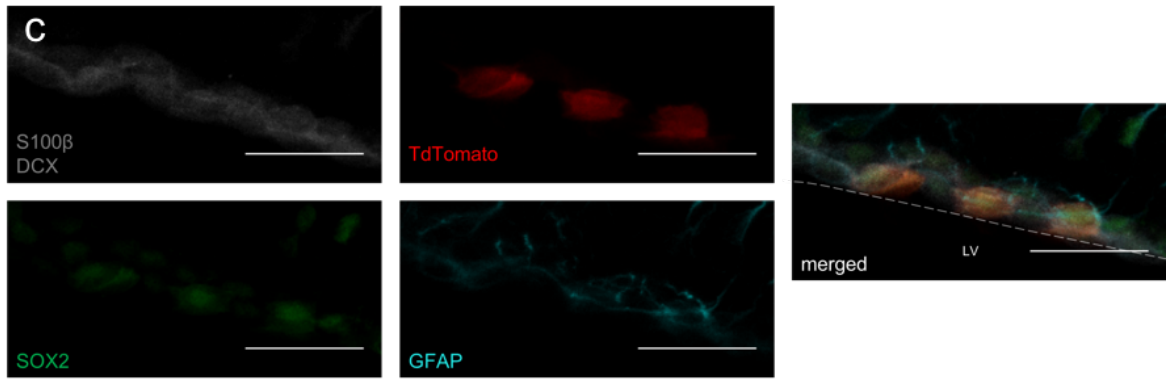
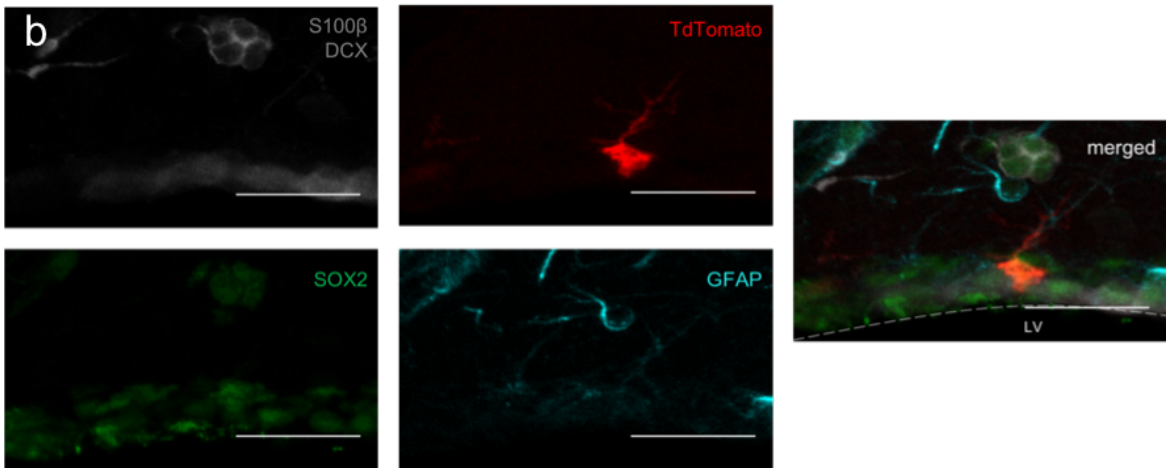
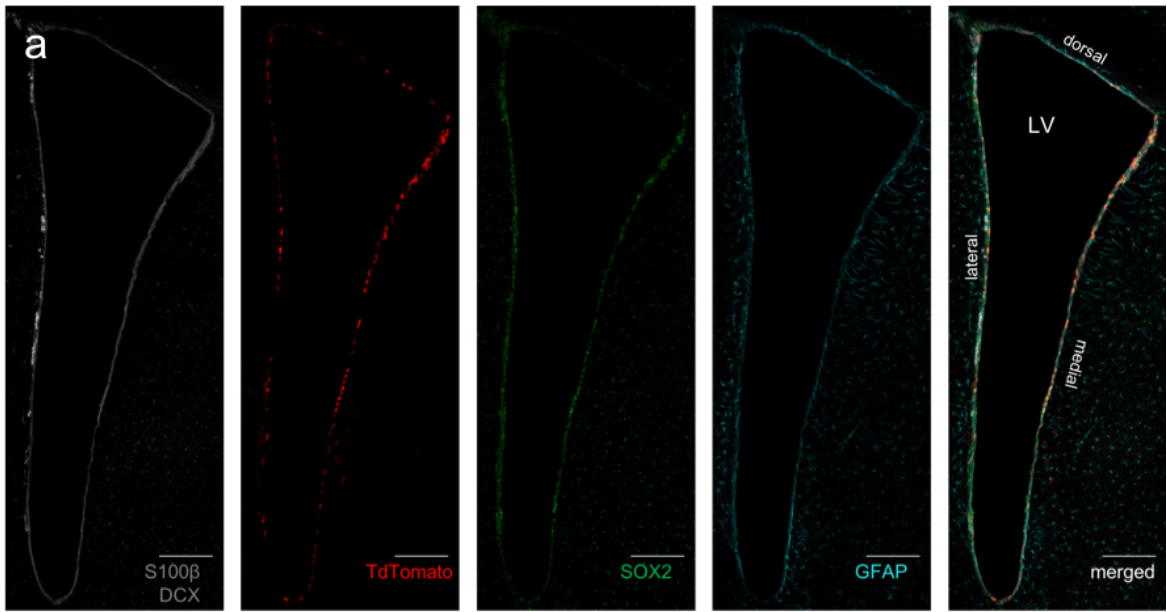
Table 8 Celltype specific markers for quantification of in vivo infection efficiency.

	S-100 β (405)	DCX (405)	SOX2 (488)	GFAP (647)
NSC			+	+
Ependymal	+		+	
Astrocyte	+		+	+
Neuroblast		+		

Five days post injection, a large number of cells were labelled along the wall of the ventricle. The labelling shows a tropism towards the medial wall of the lateral ventricle (**Figure 13a**).

After further quantification and cell type determination, approximately 10% NSCs are labelled among all cells (**Figure 14**). They are distinguished to other cell types by being SOX2 and GFAP positive, as well as by their morphology with long processes (**Figure 13b**). Almost all other labelled cells are ependymal cells, as they are S-100 β and SOX2 positive and line up along the inner wall of the ventricle (**Figure 13c**). No TdTomato positive Astrocytes (**Figure 13d**) and Neuroblasts were found.

Figure 13 (next page) Confocal images of AAV1_P5 injected ventricles 5 days post injection. Sections were immunohistochemically stained for S100 β /DCx (gray), TdTomato (red), SOX2 (green) and GFAP (cyan). **(a)** Whole view of the lateral ventricle (LV). Most cells aligning the inner ventricle wall are TdTomato positive, what indicates a successful AAV infection. Scale 150nm **(b)** Close-up on a NSC. They are identified by being SOX2 and GFAP positive and their typical processes. Scale 30nm **(c)** Close-up on ependymal cells. They are identified by being S100 β and SOX2 positive and their typical position along the inner ventricle wall. Scale 30nm **(d)** Close-up on astrocytes. They are identified by being S100 β , SOX2 and GFAP positive. Scale 20nm.



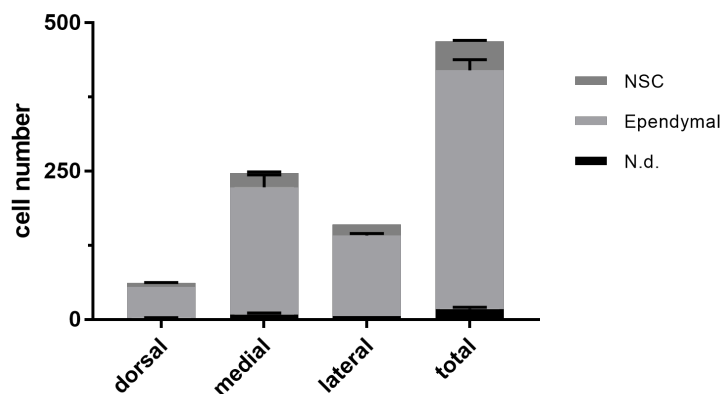


Figure 14 Celltype quantification of AAV1_P5 infected cells. Ventricles were divided in dorsal, medial and lateral wall and cells were counted using ImageJ and the parameters of Table 8. Only TdTomato positive cells were counted, as they were successfully infected with the AAV1_P5 construct. Three Sections of two mice each were analysed 5 days post injection of the virus.

3.2.2 Direct injection of Isl1 to the ventricle

After treating mice as described above (**Figure 12**), sections of one sham and one ischemia mouse were stained for DARPP-32, TdTom, and GFAP.

Sections of the sham animal show slight migration and differentiation of NSC derived progenies towards the striatum (**Figure 15a**). Those newly generated neurons stay in close proximity of the lateral wall of the ventricle.

The infection efficiency of the newly generated AAV1_P5 could be further verified, as almost all cells, regardless of the cell type, at the wall of the lateral ventricle seem to be infected and show a bright tomato signal.

After ischemia, migration of cells can be observed (**Figure 15 b,c**). Tomato positive cells can be found distal of the ventricle, just above the striatum. These cells must have their origin in the ventricle, due to their tomato signal and could be differentiated from their stem cell state, however it is more likely that they are neuroblasts on their way to the OBs. The exact cell identity is hard to determine by the staining performed.

Within the striatum, only tomato positive cell processes could be found under the microscope and no cell bodies. This is an evidence for further cell migration and differentiation.

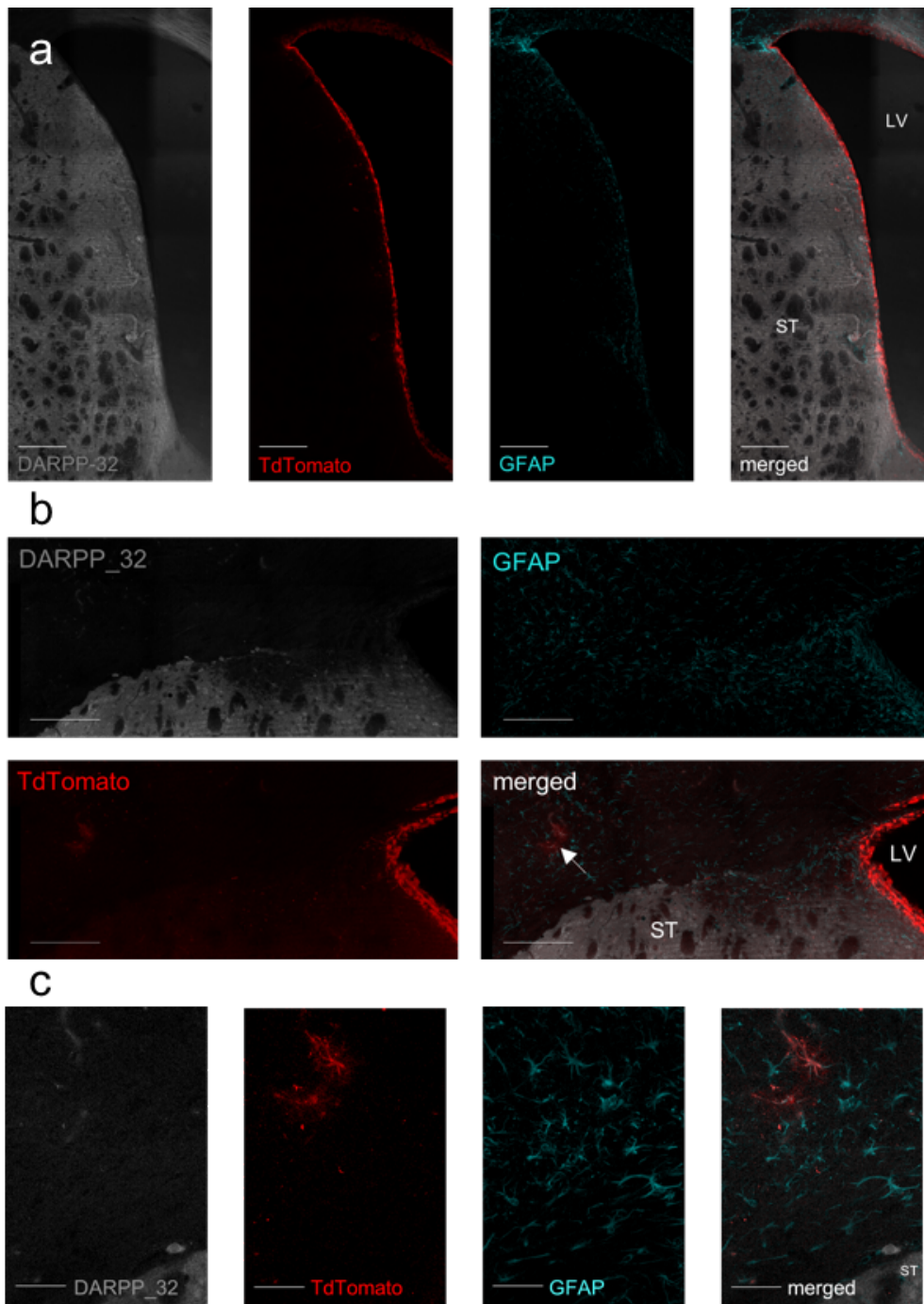


Figure 15 Confocal images 5 weeks after of directly injecting an *Isl1* overexpressing AAV1_P5 into the ventricle. Sections were immunohistochemically stained for DARPP-32 (gray), TdTomato (red) and GFAP (cyan). **(a)** Section of a Sham mouse. NSCs are found in close proximity to the lateral ventricle. Scale 200nm **(b)** Section of an injured mouse. Cells can be found distal to the lateral ventricle, dorsal of the striatum (arrow). Scale 100nm. **(c)** Close-up on migrated cells. Scale 50nm

4 Discussion

4.1 AAV efficiency

AAVs are a modern tool for gene delivery in vivo and are promising for gene therapy approaches. However, apart from their advantage of a low pathogenic profile, a mild immune response, long-term gene expression and the ability to infect dormant cells, they have some major disadvantages by today. Wild-type AAVs can infect a broad range of cells, however they are very unspecific, and the infection rate of CNS cells is 10-100 times lower compared to other organs like the liver (Bockstael et al., 2012).

Over the last decade, some researchers developed new, so called designer AAVs to specifically target the CNS (Deverman et al., 2016; Ojala et al., 2017). They could increase the infection efficiency within the CNS to over 40 times compared to the AAV9. However, they did not characterize the type of infected cells.

Here we showed that the newly generated AAV1_P5 has a tropism towards cells located in the walls of the lateral ventricle and is capable to target a high number of NSCs in the V-SVZ already after 24h, when delivered directly into the ventricle. The rapid decrease in mRNA levels after 3 days could be due to the fact that all AAV particles in the media were finally used up. As NSCs keep dividing and the AAV constructs are usually not integrating into the genome, the AAV concentration in the cell is constantly diluted so that the cells lose the AAV construct after a while.

The very different picture in the Western blot of Isl1 expression, could be because the Isl1 protein has a longer half life than its mRNA and stays in the cytoplasm even after the transcription is downregulated. Additionally, the high peak of mRNA after 3 days could be too much for the cells, leading to a feedback loop and they start downregulating it on a transcriptional level.

About 10% of all labelled cells were stem cell like (**Figure 14**). This shows an increase of about 5-7 fold compared with other, CNS specific AAVs (Kotterman et al., 2015). However, the studies were not complete by the end of this thesis and more replicates will be needed to determine a significant NSC infection efficiency. Future research will so

include the promising AAV variants from other publications and compare them to AAV9 wild-type.

4.2 Transplantation

Although, NSCs are present in the adult mammalian brain, the capacity of brain repair and adult neurogenesis remains inefficient. This could be due to the distinct regions where NSCs exist in the brain, or the microenvironment that is not supporting brain repair and NSC differentiation. To overcome these issues, we implemented a transplantation strategy for NSCs to ischemia damaged mouse brains *in vivo* (**Figure 9**). This method has been used for a variety of brain regions and showed promising results for global degenerative CNS diseases or hypoxic or ischemic encephalopathy (Gonzalez and Lee, 2016).

The NSC migration and differentiation should be increased by *Isl1*, a transcription factor that is responsible for migration and cell fate decisions in the prenatal striatum (Zhao et al., 2003). However, its exact role is still to be investigated. Here we demonstrated that transplanted cells survive the process and stay alive in the striatum for 5 weeks. The lack of *Isl1* expression after 5 weeks could be due to the long time elapsed between infection and staining. The qPCR and WB results suggest that the *Isl1* expression is downregulated after 5 to 7 days *in vitro*. This could be the reason for the lack of *Isl1* positive cells after 5 weeks in the transplantation experiment. However, because of the use of Brainbow cells, it is not clear, whether or not, the transplanted cells got infected. Those cells have an endogenous RFP signal.

Despite our hypotheses, that they will migrate towards the striatum and form new striatal neurons, they remained at the site of transplantation. This could be due to a lack of *Isl1* expression. The state of differentiation cannot be clearly determined. Considering the morphology, we suggest that the cells are in the state of a migratory, DCX positive olfactory bulb neuroblast. The fact that the cells are GFAP negative is another indicator against stem cells

This experiment was performed with an old, wild-type AAV in brainbow mice and therefore, the effective infection of NSCs could not be traced. Furthermore, *Isl1* expression could not be visualized under the microscope. For future experiments, the new AAV1_P5 will be used to induce *Isl1* expression in NSCs isolated from ischemia mice. Here, only the

infected NSCs will show a TdTomato signal and Isl1 expression can be tracked and more significant data will be generated.

4.3 Direct Injection

To minimize the cell stress and the time where NSCs are in culture medium and ex vivo, we developed an all in vivo process. Mice were injected with the Isl1 overexpressing virus directly into the ventricle, followed by BCCAO surgery 5 days post injection. They were perfused 5 weeks later and sections were stained accordingly.

In this experiment we could further confirm the promising in vitro results of the newly generated AAV1_P5 in vivo. Previous studies have shown, that with other AAV serotypes only 15%-25% among all labelled neural cells are NSCs (Kotterman et al., 2015). This numbers do not include labelled ependymal cells. Therefore, the AAV1_P5 shows an NSC labelling efficiency of more than 70% among neural cells. The tropism of the AAV towards the medial wall could be due to the flow characteristics of the CSF. As more virus particles reach the medial wall, more cells get infected.

We could show that CNS cells start migrating away from the ventricle wall upon ischemia. Those cells could be NSCs, however it is more likely that they are NSC progenies or other neuronal cell types, as NSCs normally do not migrate out of their niche. The slight migration could be triggered by the Isl1 overexpression, but it is more likely that these NSCs migrated as part of homeostasis or injury signals. This migration upon ischemia is well known and has been observed previously (Jin et al., 2003).

The migration upon Isl1 overexpression did not increase significantly and therefore the results in postnatal mice could so far not be replicated in adult mammals (Rogelius et al., 2006; Stenman et al., 2003). As the migration in ischemia induced mice was not noticeably enriched, the hypotheses that the Isl1 TFBS gets accessible through demethylation processes has to be affirmed by a more significant experimental approach.

Here, we could demonstrate that Isl1 might induce adult neurogenesis and tissue repair upon ischemia. However, it is likely that other factors will be needed to increase the migration and differentiation capacities of NSCs within the V-SVZ. Previously it has been shown that the overexpression of Isl1 combined with Neurogenin-2 can increase the

effect in postnatal mice (Rogelius et al., 2008). Ngn2 is a key factor in embryonic neurogenesis and could be the key to drive NSCs differentiation into neurons.

Future studies with a larger population of mice will bring more significant and comparable results. These results will show the real potential of Isl1 as a neurogenesis inducing factor and its potential in the regenerative field of the neurology.

References

- Allen, E. (1912). The cessation of mitosis in the central nervous system of the albino rat. cover-title, 547-568 illus., diags.
- Alonso, M., Ortega-Perez, I., Grubb, M.S., Bourgeois, J.-P., Charneau, P., and Lledo, P.-M. (2008). Turning Astrocytes from the Rostral Migratory Stream into Neurons: A Role for the Olfactory Sensory Organ. *J. Neurosci.* 28, 11089–11102.
- Altman, J. (1963). Autoradiographic investigation of cell proliferation in the brains of rats and cats. *Anat. Rec.* 145, 573–591.
- Altman, J. (1969). Autoradiographic and histological studies of postnatal neurogenesis. IV. Cell proliferation and migration in the anterior forebrain, with special reference to persisting neurogenesis in the olfactory bulb. *J. Comp. Neurol.* 137, 433–457.
- Arvidsson, A., Collin, T., Kirik, D., Kokaia, Z., and Lindvall, O. (2002). Neuronal replacement from endogenous precursors in the adult brain after stroke. *Nat. Med.* 8, 963.
- Atchison, R.W., Casto, B.C., and Hammon, W.M. (1965). Adenovirus-associated defective virus particles. *Science* (80-). 149, 754–756.
- Azevedo, F.A.C., Carvalho, L.R.B., Grinberg, L.T., Farfel, J.M., Ferretti, R.E.L., Leite, R.E.P., Filho, W.J., Lent, R., and Herculano-Houzel, S. (2009). Equal numbers of neuronal and nonneuronal cells make the human brain an isometrically scaled-up primate brain. *J. Comp. Neurol.* 513, 532–541.
- Basak, O., Krieger, T.G., Muraro, M.J., Wiebrands, K., Stange, D.E., Frias-Aldeguer, J., Rivron, N.C., van de Wetering, M., van Es, J.H., van Oudenaarden, A., et al. (2018). Troy+ brain stem cells cycle through quiescence and regulate their number by sensing niche occupancy. *Proc. Natl. Acad. Sci.* 201715911.
- Beckervordersandforth, R., Tripathi, P., Ninkovic, J., Bayam, E., Lepier, A., Stempfhuber, B., Kirchhoff, F., Hirrlinger, J., Haslinger, A., Lie, D.C., et al. (2017). In Vivo Fate Mapping and Expression Analysis Reveals Molecular Hallmarks of Prospectively Isolated Adult Neural Stem Cells. *Cell Stem Cell* 7, 744–758.
- Benner, E.J., Luciano, D., Jo, R., Abdi, K., Paez-Gonzalez, P., Sheng, H., Warner, D., Liu, C.,

- Eroglu, C., and Kuo, C.T. (2013). Post-injury protective astrogenesis from SVZ niche is controlled by Notch modulator Thbs4. *Nature* 497, 369–373.
- Bergmann, O., Liebl, J., Bernard, S., Alkass, K., Yeung, M.S.Y., Steier, P., Kutschera, W., Johnson, L., Landén, M., Druid, H., et al. (2012). The Age of Olfactory Bulb Neurons in Humans. *Neuron* 74, 634–639.
- Bobadilla, E.L. (2016). Molecular and Cellular Determinants of Injury-induced Neurogenesis. Ruperto-Carola University of Heidelberg.
- Bockstael, O., Foust, K.D., Kaspar, B., and Tenenbaum, L. (2012). Recombinant AAV Delivery to the Central Nervous System. R.O. Snyder, and P. Moullier, eds. (Totowa, NJ: Humana Press), pp. 159–177.
- Brown, J.P., Couillard-Després, S., Cooper-Kuhn, C.M., Winkler, J., Aigner, L., and Kuhn, H.G. (2003). Transient expression of doublecortin during adult neurogenesis. *J. Comp. Neurol.* 467, 1–10.
- Buecker, C., and Wsocka, J. (2012). Enhancers as information integration hubs in development: lessons from genomics. *Trends Genet.* 28, 276–284.
- Calcedo, R., Morizono, H., Wang, L., McCarter, R., He, J., Jones, D., Batshaw, M.L., and Wilson, J.M. (2011). Adeno-associated virus antibody profiles in newborns, children, and adolescents. *Clin. Vaccine Immunol.* 18, 1586–1588.
- Chang, L.S., Shi, Y., and Shenk, T. (1989). Adeno-associated virus P5 promoter contains an adenovirus E1A-inducible element and a binding site for the major late transcription factor. *J Virol* 63, 3479–3488.
- Collin, T., Arvidsson, A., Kokaia, Z., and Lindvall, O. (2005). Quantitative analysis of the generation of different striatal neuronal subtypes in the adult brain following excitotoxic injury. *Exp. Neurol.* 195, 71–80.
- Custo Greig, L.F., Woodworth, M.B., Galazo, M.J., Padmanabhan, H., and Macklis, J.D. (2013). Molecular logic of neocortical projection neuron specification, development and diversity. *Nat. Rev. Neurosci.* 14, 10.1038/nrn3586.
- Deverman, B.E., Pravdo, P.L., Simpson, B.P., Kumar, S.R., Chan, K.Y., Banerjee, A., Wu, W.-

- L., Yang, B., Huber, N., Pasca, S.P., et al. (2016). Cre-dependent selection yields AAV variants for widespread gene transfer to the adult brain. *Nat. Biotechnol.* *34*, 204–209.
- Doetsch, F., García-Verdugo, J.M., and Alvarez-Buylla, A. (1997). Cellular Composition and Three-Dimensional Organization of the Subventricular Germinal Zone in the Adult Mammalian Brain. *J. Neurosci.* *17*, 5046 LP-5061.
- Ellis, P., Fagan, B.M., Magness, S.T., Hutton, S., Taranova, O., Hayashi, S., McMahon, A., Rao, M., and Pevny, L. (2004). SOX2, a Persistent Marker for Multipotential Neural Stem Cells Derived from Embryonic Stem Cells, the Embryo or the Adult. *Dev. Neurosci.* *26*, 148–165.
- Ernst, A., Alkass, K., Bernard, S., Salehpour, M., Perl, S., Tisdale, J., Possnert, G., Druid, H., and Fris??n, J. (2014). Neurogenesis in the striatum of the adult human brain. *Cell* *156*, 1072–1083.
- Gonzalez, R., and Lee, M.H.H. and J.-P. (2016). Neural Stem Cell Transplantation and CNS Diseases. *CNS Neurol. Disord. - Drug Targets* *15*, 881–886.
- Götz, M., and Barde, Y.A. (2005). Radial glial cells: Defined and major intermediates between embryonicstem cells and CNS neurons. *Neuron* *46*, 369–372.
- Grimm, D., Kern, A., Rittner, K., and Kleinschmidt, J.A. (1998). Novel tools for production and purification of recombinant adenoassociated virus vectors. *Hum. Gene Ther.* *9*, 2745–2760.
- Gusel'nikova, V. V., and Korzhevskiy, D.E. (2015). NeuN as a neuronal nuclear antigen and neuron differentiation marker. *Acta Naturae* *7*, 42–47.
- Hirose, K., Shimoda, N., and Kikuchi, Y. (2013). Transient reduction of 5-methylcytosine and 5-hydroxymethylcytosine is associated with active DNA demethylation during regeneration of zebrafish fin. *Epigenetics* *8*, 899–906.
- Hon, G.C., Rajagopal, N., Shen, Y., McCleary, D.F., Yue, F., Dang, M.D., and Ren, B. (2013). Epigenetic memory at embryonic enhancers identified in DNA methylation maps from adult mouse tissues. *Nat. Genet.* *45*, 1198.
- Howard, P.W., and Maurer, R.A. (2000). Identification of a conserved protein that interacts with specific LIM homeodomain transcription factors. *J. Biol. Chem.* *275*, 13336–13342.

- Hunter, C.S., and Rhodes, S.J. (2005). LIM-homeodomain genes in mammalian development and human disease. *Mol. Biol. Rep.* 32, 67–77.
- Ihrle, R.A., and Álvarez-Buylla, A. (2011). Lake-Front Property: A Unique Germinal Niche by the Lateral Ventricles of the Adult Brain. *Neuron* 70, 674–686.
- Jagannathan, B., Elms, P.J., Bustamante, C., and Marqusee, S. (2012). Direct observation of a force-induced switch in the anisotropic mechanical unfolding pathway of a protein. *Proc. Natl. Acad. Sci.* 109, 17820–17825.
- Janik, J.E., Huston, M.M., and Rose, J. a (1981). Locations of adenovirus genes required for the replication of adenovirus-associated virus. *Proc. Natl. Acad. Sci. U. S. A.* 78, 1925–1929.
- Jin, K., Sun, Y., Xie, L., Peel, A., Mao, X.O., Batteur, S., and Greenberg, D.A. (2003). Directed migration of neuronal precursors into the ischemic cerebral cortex and striatum. *Mol. Cell. Neurosci.* 24, 171–189.
- Kempermann, G., Chesler, E.J., Lu, L., Williams, R.W., and Gage, F.H. (2006). Natural variation and genetic covariance in adult hippocampal neurogenesis. *Proc. Natl. Acad. Sci. U. S. A.* 103, 780–785.
- Kohwi, M., Petryniak, M.A., Long, J.E., Ekker, M., Obata, K., Yanagawa, Y., Rubenstein, J.L.R., and Alvarez-Buylla, A. (2007). A Subpopulation of Olfactory Bulb GABAergic Interneurons Is Derived from Emx1- and Dlx5/6-Expressing Progenitors. *J. Neurosci.* 27, 6878–6891.
- Kotterman, M.A., Vazin, T., and Schaffer, D. V (2015). Enhanced selective gene delivery to neural stem cells in vivo by an adeno-associated viral variant. *Development* 142, 1885–1892.
- Kriegstein, A., and Alvarez-Buylla, A. (2011). The Glial Nature of Embryonic and Adult Neural Stem Cells. *Annu. Rev. Neurosci.* 149–184.
- Kyritsis, N., Kizil, C., and Brand, M. (2014). Neuroinflammation and central nervous system regeneration in vertebrates. *Trends Cell Biol.* 24, 128–135.
- Lee, J., Sayed, N., Hunter, A., Au, K.F., Wong, W.H., Edward, S., Pera, R.R., Yakubov, E., and Cooke, J.P. (2013). Activation of Innate Immunity is Required for Efficient Nuclear Reprogramming. *Cell* 151, 547–558.

- Lim, D.A., and Alvarez-Buylla, A. (2014). Adult neural stem cells stake their ground. *Trends Neurosci.* *37*, 563–571.
- Liu, F., You, Y., Li, X., Ma, T., Nie, Y., Wei, B., Li, T., Lin, H., and Yang, Z. (2009). Brain Injury Does Not Alter the Intrinsic Differentiation Potential of Adult Neuroblasts. *J. Neurosci.* *29*, 5075–5087.
- Lledo, P.-M., Alonso, M., and Grubb, M.S. (2006). Adult neurogenesis and functional plasticity in neuronal circuits. *Nat. Rev. Neurosci.* *7*, 179.
- Lledo, P.M., Merkle, F.T., and Alvarez-Buylla, A. (2008). Origin and function of olfactory bulb interneuron diversity. *Trends Neurosci.* *31*, 392–400.
- Llorens-Bobadilla, E., Zhao, S., Baser, A., Saiz-Castro, G., Zwadlo, K., and Martin-Villalba, A. (2015). Single-Cell Transcriptomics Reveals a Population of Dormant Neural Stem Cells that Become Activated upon Brain Injury. *Cell Stem Cell* *17*, 329–340.
- Lois, C., García-Verdugo, J.-M., and Alvarez-Buylla, A. (1996). Chain Migration of Neuronal Precursors. *Science* (80-.). *271*, 978 LP-981.
- Massalini, S., Pellegatta, S., Pisati, F., Finocchiaro, G., Farace, M.G., and Ciafrè, S.A. (2009). Reelin affects chain-migration and differentiation of neural precursor cells. *Mol. Cell. Neurosci.* *42*, 341–349.
- Matsushita, T., Elliger, S., Elliger, C., Podsakoff, G., Villarreal, L., Kurtzman, G.J., Iwaki, Y., and Colosi, P. (1998). Adeno-associated virus vectors can be efficiently produced without helper virus. *Gene Ther.* *5*, 938–945.
- McLaughlin, S.K., Collis, P., Hermonat, P.L., and Muzyczka, N. (1988). Adeno-associated virus general transduction vectors: analysis of proviral structures. *J. Virol.* *62*, 1963–1973.
- Merkle, F.T., Fuentealba, L.C., Sanders, T.A., Magno, L., Kessar, N., and Alvarez-Buylla, A. (2013). Adult neural stem cells in distinct microdomains generate previously unknown interneuron types. *Nat. Neurosci.* *17*, 207–214.
- Michelsen, J.W., Schmeichel, K.L., Beckerle, M.C., and Winge, D.R. (1993). The LIM motif defines a specific zinc-binding protein domain. *Proc. Natl. Acad. Sci.* *90*, 4404–4408.

- Ming, G. li, and Song, H. (2011). Adult Neurogenesis in the Mammalian Brain: Significant Answers and Significant Questions. *Neuron* 70, 687–702.
- Mirzadeh, Z., Doetsch, F., Sawamoto, K., Wichterle, H., and Alvarez-Buylla, A. (2010). The Subventricular Zone En-face: Wholemount Staining and Ependymal Flow. *J. Vis. Exp.* 1–8.
- Nakafuku, M., and Grande, A. (2013). Neurogenesis in the Damaged Mammalian Brain. In *Comprehensive Developmental Neuroscience: Patterning and Cell Type Specification in the Developing CNS and PNS*, (Elsevier), pp. 551–608.
- Nakatomi, H., Kuriu, T., Okabe, S., Yamamoto, S. ichi, Hatano, O., Kawahara, N., Tamura, A., Kirino, T., and Nakafuku, M. (2002). Regeneration of hippocampal pyramidal neurons after ischemic brain injury by recruitment of endogenous neural progenitors. *Cell* 110, 429–441.
- Ni, T.H., McDonald, W.F., Zolotukhin, I., Melendy, T., Waga, S., Stillman, B., and Muzyczka, N. (1998). Cellular proteins required for adeno-associated virus DNA replication in the absence of adenovirus coinfection. *J. Virol.* 72, 2777–2787.
- Obernier, K., Cebrian-Silla, A., Thomson, M., Parraguez, J.I., Anderson, R., Guinto, C., Rodas Rodriguez, J., Garcia-Verdugo, J.-M., and Alvarez-Buylla, A. (2018). Adult Neurogenesis Is Sustained by Symmetric Self-Renewal and Differentiation. *Cell Stem Cell* 22, 221–234.e8.
- Ojala, D.S., Sun, S., Santiago-Ortiz, J.L., Shapiro, M.G., Romero, P.A., and Schaffer, D. V. (2017). In Vivo Selection of a Computationally Designed SCHEMA AAV Library Yields a Novel Variant for Infection of Adult Neural Stem Cells in the SVZ. *Mol. Ther.*
- Okada, T. (2013). Efficient AAV Vector Production System: Towards Gene Therapy For Duchenne Muscular Dystrophy. F.M.B.T.-G.T.-T. and P.A. Molina, ed. (Rijeka: InTech), p. Ch. 17.
- Picelli, S., Faridani, O.R., Björklund, Å.K., Winberg, G., Sagasser, S., and Sandberg, R. (2014). Full-length RNA-seq from single cells using Smart-seq2. *Nat. Protoc.* 9, 171–181.
- Ponti, G., Obernier, K., and Alvarez-Buylla, A. (2013). Lineage progression from stem cells to new neurons in the adult brain ventricular-subventricular zone. *Cell Cycle* 12, 1649–1650.
- Rayaprolu, V., Kruse, S., Kant, R., Venkatakrishnan, B., Movahed, N., Brooke, D., Lins, B., Bennett, A., Potter, T., McKenna, R., et al. (2013). Comparative Analysis of Adeno-Associated

Virus Capsid Stability and Dynamics. *J. Virol.* *87*, 13150–13160.

Rogelius, N., Jensen, J.B., Lundberg, C., and Parmar, M. (2006). Retrovirally delivered Islet-1 increases recruitment of Ng2 expressing cells from the postnatal SVZ into the striatum. *Exp. Neurol.* *201*, 388–398.

Rogelius, N., Hebsgaard, J.B., Lundberg, C., and Parmar, M. (2008). Reprogramming of neonatal SVZ progenitors by Islet-1 and Neurogenin-2. *Mol. Cell. Neurosci.* *38*, 453–459.

Samulski, R.J., and Muzyczka, N. (2014). AAV-Mediated Gene Therapy for Research and Therapeutic Purposes. *Annu. Rev. Virol.* *1*, 427–451.

Samulski, R.J., Chang, L.S., and Shenk, T. (1989). Helper-free stocks of recombinant adeno-associated viruses: normal integration does not require viral gene expression. *J. Virol.* *63*, 3822–3828.

Sánchez-García, I., and Rabbits, T.H. (1994). The LIM domain: a new structural motif found in zinc-finger-like proteins. *Trends Genet.* *10*, 315–320.

Slanina, H., Weger, S., Stow, N.D., Kuhrs, A., and Heilbronn, R. (2006). Role of the herpes simplex virus helicase-primase complex during adeno-associated virus DNA replication. *J. Virol.* *80*, 5241–5250.

Smith, R.H., Levy, J.R., and Kotin, R.M. (2009). A simplified baculovirus-AAV expression vector system coupled with one-step affinity purification yields high-titer rAAV stocks from insect cells. *Mol. Ther.* *17*, 1888–1896.

Sonntag, F., Schmidt, K., and Kleinschmidt, J.A. (2010). A viral assembly factor promotes AAV2 capsid formation in the nucleolus. *Proc. Natl. Acad. Sci.* *107*, 10220–10225.

Speetzen, L.J., Endres, M., and Kunz, A. (2013). Bilateral Common Carotid Artery Occlusion as an Adequate Preconditioning Stimulus to Induce Early Ischemic Tolerance to Focal Cerebral Ischemia. *J. Vis. Exp.* 1–7.

Stenman, J., Toresson, H., and Campbell, K. (2003). Identification of two distinct progenitor populations in the lateral ganglionic eminence: implications for striatal and olfactory bulb neurogenesis. *J. Neurosci.* *23*, 167–174.

- Strobel, B., Miller, F.D., Rist, W., and Lamla, T. (2015). Comparative Analysis of Cesium Chloride- and Iodixanol-Based Purification of Recombinant Adeno-Associated Viral Vectors for Preclinical Applications. *Hum. Gene Ther. Methods* 26, 147–157.
- Svenningsson, P., Nishi, A., Fisone, G., Girault, J.-A., Nairn, A.C., and Greengard, P. (2004). DARPP-32: An Integrator of Neurotransmission. *Annu. Rev. Pharmacol. Toxicol.* 44, 269–296.
- Tanaka, E.M., and Ferretti, P. (2009). Considering the evolution of regeneration in the central nervous system. *Nat. Rev. Neurosci.* 10, 713–723.
- Wang, H.F., and Liu, F.C. (2001). Developmental restriction of the LIM homeodomain transcription factor Islet-1 expression to cholinergic neurons in the rat striatum. *Neuroscience* 103, 999–1016.
- Wang, Q., Gu, L., Adey, A., Radlwimmer, B., Wang, W., Hovestadt, V., Bähr, M., Wolf, S., Shendure, J., Eils, R., et al. (2013). Tagmentation-based whole-genome bisulfite sequencing. *Nat. Protoc.* 8, 2022.
- Wu, Z., Yang, H., and Colosi, P. (2010). Effect of genome size on AAV vector packaging. *Mol. Ther.* 18, 80–86.
- Xie, Q., Bu, W., Bhatia, S., Hare, J., Somasundaram, T., Azzi, A., and Chapman, M.S. (2002). The atomic structure of adeno-associated virus (AAV-2), a vector for human gene therapy. *Proc. Natl. Acad. Sci. U. S. A.* 99, 10405–10410.
- Zhao, Y., Marin, O., Hermes, E., Powell, A., Flames, N., Palkovits, M., Rubenstein, J.L.R., and Westphal, H. (2003). The LIM-homeobox gene Lhx8 is required for the development of many cholinergic neurons in the mouse forebrain. *Proc. Natl. Acad. Sci.* 100, 9005–9010.
- Zhou, X., Zeng, X., Fan, Z., Li, C., McCown, T., Samulski, R.J., and Xiao, X. (2008). Adeno-associated virus of a single-polarity DNA genome is capable of transduction in vivo. *Mol. Ther.* 16, 494–499.
- Zhuang, S., Zhang, Q., Zhuang, T., Evans, S.M., Liang, X., and Sun, Y. (2013). Expression of Isl1 during mouse development. *Gene Expr. Patterns* 13, 407–412.